



APPROVED FOR PUBLIC RELEASE, DISTRIBUTION UNLIMITED

ALEX(01)-TR-78-82

LEVEL

12

EXTRACTION OF SEISMIC WAVEFORMS

AD A0 66711

TECHNICAL REPORT NO. 14
VELA NETWORK EVALUATION AND AUTOMATIC PROCESSING RESEARCH

Prepared by
Alan C. Strauss

TEXAS INSTRUMENTS INCORPORATED
Equipment Group
Post Office Box 6015
Dallas, Texas 75222

DDC
REFMIP
APR 2 1978
REGISTRATION
C

Prepared for
AIR FORCE TECHNICAL APPLICATIONS CENTER
Alexandria, Virginia 22314

Sponsored by
ADVANCED RESEARCH PROJECTS AGENCY
Nuclear Monitoring Research Office
ARPA Program Code No. 7F10
ARPA Order No. 2551

29 September 1978

DDC FILE COPY

Acknowledgment: This research was supported by the Advanced Research Projects Agency, Nuclear Monitoring Research Office, under Project VELA-UNIFORM, and accomplished under the technical direction of the Air Force Technical Applications Center at the Contract Number F49620-77-C-0004.

19 04 02 1978



APPROVED FOR PUBLIC RELEASE, DISTRIBUTION UNLIMITED

ALEX(01)-TR-78-02

EXTRACTION OF SEISMIC WAVEFORMS

**TECHNICAL REPORT NO. 14
VELA NETWORK EVALUATION AND AUTOMATIC PROCESSING RESEARCH**

Prepared by
Alan C. Strauss

TEXAS INSTRUMENTS INCORPORATED
Equipment Group
Post Office Box 6015
Dallas, Texas 75222



Prepared for
AIR FORCE TECHNICAL APPLICATIONS CENTER
Alexandria, Virginia 22314

Sponsored by
ADVANCED RESEARCH PROJECTS AGENCY
Nuclear Monitoring Research Office
ARPA Program Code No. 7F10
ARPA Order No. 2551

29 September 1978

Acknowledgment: This research was supported by the Advanced Research Projects Agency, Nuclear Monitoring Research Office, under Project VELA-UNIFORM, and accomplished under the technical direction of the Air Force Technical Applications Center under Contract Number F08606-77-C-0004.

Equipment Group

UNCLASSIFIED

SECURITY CLASSIFICATION OF THIS PAGE (When Data Entered)

REPORT DOCUMENTATION PAGE		READ INSTRUCTIONS BEFORE COMPLETING FORM
1. REPORT NUMBER	2. GOVT ACCESSION NO.	3. RECIPIENT'S CATALOG NUMBER
4. TITLE (and Subtitle) EXTRACTION OF SEISMIC WAVEFORMS VELA Network Evaluation and Automatic		5. TYPE OF REPORT & PERIOD COVERED 9 Technical rept. no. 14
10 Alan C. Strauss		6. PERFORMING ORG. REPORT NUMBER ALEX(01)-TR-78-02
9. PERFORMING ORGANIZATION NAME AND ADDRESS Texas Instruments Incorporated Equipment Group Dallas, Texas 75222		7. CONTRACT OR GRANT NUMBER(s) F08606-77-C-0004 ARPA Order-2551
11. CONTROLLING OFFICE NAME AND ADDRESS Advanced Research Projects Agency Nuclear Monitoring Research Office Arlington, Virginia 22209		12. REPORT DATE 29 Sep 1978
14. MONITORING AGENCY NAME & ADDRESS (if different from Controlling Office) Air Force Technical Applications Center VELA Seismological Center Alexandria, Virginia 22314		13. NUMBER OF PAGES 72
15. SECURITY CLASS. (of this report) UNCLASSIFIED		15a. DECLASSIFICATION/DOWNGRADING SCHEDULE
16. DISTRIBUTION STATEMENT (of this Report) APPROVED FOR PUBLIC RELEASE, DISTRIBUTION UNLIMITED		
17. DISTRIBUTION STATEMENT (of the abstract entered in Block 20, if different from Report)		
18. SUPPLEMENTARY NOTES ARPA Order No. 2551		
19. KEY WORDS (Continue on reverse side if necessary and identify by block number) Seismology Polarization filter Angle of incidence Bodywaves Detection thresholds Wiener filter Surface waves M _s - m _b relationships Bandpass filter Signal extraction Cascaded processor Three-component adaptive processing		
20. ABSTRACT (Continue on reverse side if necessary and identify by block number) This report considers the effects on detectability and measurability resulting from attempts to extract seismic waveforms by application of cascaded processors and polarization filters. Previous work has shown that bandpass or Wiener filters (when cascaded with the three-component surface wave adaptive processor) caused improvements of as much as 0.8 m _b units in the 50 percent detection threshold of surface waves. This report shows that by using a larger data base, this improvement in the detection threshold		

DD FORM 1 JAN 73 1473

EDITION OF 1 NOV 65 IS OBSOLETE

UNCLASSIFIED

SECURITY CLASSIFICATION OF THIS PAGE (When Data Entered)

405 076

SW

m sub 8

over

UNCLASSIFIED

SECURITY CLASSIFICATION OF THIS PAGE(When Data Entered)

20. continued

is 0.5 units. It is also shown in this report that surface wave magnitudes measured on data processed by the bandpass filter-three-component surface wave adaptive processor cascaded combination compare well with surface wave magnitudes measured on bandpass filtered data, however, surface wave magnitudes measured on data processed by the Wiener filter-three-component surface wave adaptive processor do not.

Two types of polarization filters are described in this report. The first, which is dependent on vertical and radial component particle motion, improves the long-period 50 percent detection threshold by 0.3 m_p units for P waves and 0.4 m_p units for S waves when applied to Kurile Island, Kamchatka events as recorded at Mashhad. The second, which is dependent on phase difference between the vertical and radial data, improves the long-period 50 percent detection threshold by approximately 0.5 m_p units for P and S waves. Discussion on the feasibility of applying these polarization filters to short-period data is also presented.

UNCLASSIFIED

SECURITY CLASSIFICATION OF THIS PAGE(When Data Entered)

ABSTRACT

This report considers the effects on detectability and measurability resulting from attempts to extract seismic waveforms by application of cascaded processors and polarization filters. Previous work has shown that bandpass or Wiener filters (when cascaded with the three-component surface wave adaptive processor) caused improvements of as much as $0.8 m_b$ units in the 50 percent detection threshold of surface waves. This report shows that by using a larger data base, this improvement in the detection threshold is 0.5 units. It is also shown in this report that surface wave magnitudes measured on data processed by the bandpass filter-three-component surface wave adaptive processor cascaded combination compare well with surface wave magnitudes measured on bandpass filtered data, however, surface wave magnitudes measured on data processed by the Wiener filter-three-component surface wave adaptive processor do not.

Two types of polarization filters are described in this report. The first, which is dependent on vertical and radial component particle motion, improves the long-period 50 percent detection threshold by $0.3 m_b$ units for P waves and $0.4 m_b$ units for S waves when applied to Kurile Island, Kamchatka events as recorded at Mashhad. The second, which is dependent on phase difference between the vertical and radial data, improves the long-period 50 percent detection threshold by approximately $0.5 m_b$ units for P and S waves. Discussion on the feasibility of applying these polarization filters to short-period data is also presented.

ACCESSION for	White Section <input checked="" type="checkbox"/>	Buff Section <input type="checkbox"/>
NTIS		
DOC		
UNANNOUNCED		
JUSTIFICATION		
BY	DISTRICT HEADQUARTERS, SPECIAL	
	A	

TABLE OF CONTENTS

SECTION	TITLE	PAGE
	ABSTRACT	iii
I.	INTRODUCTION	I-1
II.	METHODOLOGY	II-1
	A. THE GENERALIZED APPROACH TO SIGNAL EXTRACTION	II-1
	B. SIGNAL EXTRACTION TECHNIQUES	II-6
	C. FINAL COMMENTS ON THE METHODOLOGY OF THE EVALUATION OF SIGNAL EXTRAC- TION TECHNIQUES	II-11
III.	DATA ANALYSIS	III-1
	A. EXTRACTION OF LONG-PERIOD SURFACE WAVES BY CASCADED PROCESSORS	III-1
	B. EXTRACTION OF LONG-PERIOD BODY- WAVES BY PARTICLE-MOTION POLARIZA- TION FILTERS	III-13
	C. EXTRACTION OF SHORT-PERIOD BODY- WAVES BY PARTICLE-MOTION POLARIZA- TION FILTERS	III-21
	D. EXTRACTION OF LONG-PERIOD SIGNALS BY PHASE-DIFFERENCE POLARIZATION FILTERS	III-28
	E. EXTRACTION OF SHORT-PERIOD SIGNALS BY PHASE-DIFFERENCE POLARIZATION FILTERS	III-37
	F. FINAL COMMENTS	III-39

TABLE OF CONTENTS
(continued)

SECTION	TITLE	PAGE
IV.	CONCLUSIONS & RECOMMENDATIONS	IV-1
	A. CONCLUSIONS DRAWN FROM THIS STUDY	IV-1
	B. RECOMMENDATIONS FOR FUTURE WORK	IV-3
V.	REFERENCES	V-1

LIST OF FIGURES

FIGURE	TITLE	PAGE
II-1	TRAPEZOIDAL FILTER WEIGHT SCHEME	II-4
II-2	THE GENERALIZED PROCESSING SCHEME	II-5
III-1	TYPICAL DATA OUTPUT BY CASCADED PROCESSORS	III-2
III-2	SURFACE WAVE EXTRACTION DETECTION STATISTICS	III-4
III-3	$M_g - m_b$ DATA MEASURED ON THE VERTICAL COMPONENT AT 20-SECONDS PERIOD AFTER BANDPASS FILTERING	III-7
III-4	$M_g - m_b$ DATA MEASURED ON THE VERTICAL COMPONENT AT 20-SECONDS PERIOD AFTER BPF-TSCWA CASCADED PROCESSING	III-8
III-5	$M_g - m_b$ DATA MEASURED ON THE VERTICAL COMPONENT AT 20-SECONDS PERIOD AFTER WF-TCSWA CASCADED PROCESSING	III-9
III-6	SAMPLE OUTPUTS FROM PARTICLE-MOTION POLARIZATION FILTER	III-14
III-7	REFLECTION AND REFRACTION OF P WAVES AT AN INTERFACE BETWEEN TWO ELASTIC SOLIDS	III-16
III-8	DETECTION STATISTICS MEASURED ON BANDPASS FILTERED BODYWAVES-MASHHAD-KURILE ISLANDS KAMCHATKA DATA BASE	III-18
III-9	DETECTION STATISTICS MEASURED ON PARTICLE-MOTION POLARIZATION FILTERED BODYWAVES-MASHHAD-KURILE ISLANDS, KAMCHATKA DATA BASE	III-19
III-10	MEASURABILITY OF P WAVES PROCESSED BY THE PARTICLE-MOTION POLARIZATION FILTER	III-22
III-11	TRAVEL PATHS OF P_n , P^* , AND P_g (MODIFIED FROM RICHTER, 1958)	III-24

LIST OF FIGURES
(continued)

FIGURE	TITLE	PAGE
III-12	SAMPLE OUTPUT FROM SHORT-PERIOD PARTICLE-MOTION POLARIZATION FILTER PROGRAM APPLIED TO A NEAR-FIELD ($\Delta = 5.84^\circ$) EVENT	III-25
III-13	SAMPLE OUTPUT FROM SHORT-PERIOD PARTICLE-MOTION POLARIZATION FILTER PROGRAM APPLIED TO A TELESEISMIC ($\Delta = 21.17^\circ$) EVENT	III-27
III-14	SAMPLE OUTPUT FROM THE PHASE-DIFFER- ENCE POLARIZATION FILTER PROGRAM USING A 32 POINT PROCESSING SEGMENT	III-29
III-15	SAMPLE OUTPUT FROM THE PHASE-DIFFER- ENCE POLARIZATION FILTER PROGRAM USING A 64 POINT PROCESSING SEGMENT	III-30
III-16	SCALED-UP PLOT OF THE BODYWAVE DATA OF FIGURES III-13 AND III-14	III-32
III-17	DETECTION STATISTICS MEASURED ON PHASE- DIFFERENCE POLARIZATION FILTERED BODY- WAVES-MASHHAD-KURILE ISLANDS, KAMCHATKA DATA BASE	III-35
III-18	MEASURABILITY OF P WAVES PROCESSED BY THE PHASE-DIFFERENCE POLARIZATION FILTER	III-36
III-19	SAMPLE SHORT-PERIOD NEAR-FIELD EVENT PROCESSED BY THE PHASE-DIFFERENCE POLARIZATION FILTER	III-38
III-20	SAMPLE SHORT-PERIOD TELESEISMIC P WAVE DATA PROCESSED BY THE PHASE-DIFFERENCE POLARIZATION FILTER	III-40

LIST OF TABLES

TABLE	TITLE	PAGE
III-1	SUMMARY OF SURFACE WAVE DETECTION STATISTICS	III-5
III-2	$M_s - m_b$ RELATIONSHIPS FOR DATA OF FIGURES III-3 THROUGH III-5	III-11
III-3	COMPARISON OF BANDPASS FILTER AND PARTICLE-MOTION POLARIZATION FILTER DETECTION THRESHOLDS FOR LONG-PERIOD MASHHAD-RECORDED EVENTS	III-20
III-4	COMPARISON OF BANDPASS FILTER AND PHASE DIFFERENCE POLARIZATION FILTER DETECTION THRESHOLDS FOR LONG-PERIOD MASHHAD-RECORDED EVENTS	III-34

SECTION I INTRODUCTION

The research effort which this report describes was initially intended to clear up several points raised at the end of the previous contract period regarding the extraction of teleseismic long-period bodywaves and surface waves from seismic noise. A further point to be covered was the logical extension of the signal extraction techniques used on teleseismic long-period data to extraction of short-period waveforms from near-field data. During the course of this work, however, a new, and potentially more useful, signal extraction technique was developed from a synthesis of previously used techniques. Therefore, in addition to describing the results of the work performed to achieve the original goals, a discussion of the new technique (hereafter to be referred to as the phase-difference polarization filter) and preliminary evaluation of its usefulness is included in this report.

Lane (1977a) demonstrated that polarization filters (hereafter to be referred to as particle-motion polarization filters) yielded essentially no improvement in station detection capability of long-period teleseismic signals. It is therefore necessary to determine why these particle-motion polarization filters performed so poorly on the chosen data base and whether this technique might perform better for a different station-source region combination.

In the area of long-period surface wave extraction, Lane (1977b) demonstrated that by cascading signal processing techniques (i. e. , using as input to one processor the output of another processor) greater signal-to-noise ratio improvements could be achieved than would be expected from the signal-to-noise ratio improvement yielded by each technique when applied separately.

Due to the size of the data base available at the time of analysis, Lane was only able to conclude that the improvement in detection capability due to use of cascaded signal extraction techniques might be as large as 0.8 m_b units for Kurile Islands-Kamchatka events as recorded at the Guam Seismic Research Observatory. By expanding the data base, it is intended in this report to better define the detection capability improvement due to application of cascaded signal extraction techniques. By applying Ringdal's method for magnitude bias correction (Ringdal, 1975; Strauss, 1978) it is possible to investigate the effects on the $M_s - m_b$ relationship of extending the detection capability of a station by the cascade method.

The specific goals of this report are as follows:

- To investigate the failure of the particle-motion polarization filter to improve the Guam SRO detection capability of Kurile Islands-Kamchatka events.
- To determine the value of particle-motion polarization filters when applied to teleseismic signals recorded at another station.
- To investigate the feasibility of applying particle-motion polarization filters to short-period near-field data.
- To obtain better estimates of the detection capability improvement due to the application of cascaded signal extraction techniques to long-period surface wave data.
- To determine the effects on the $M_s - m_b$ relationship of cascaded signal extraction techniques.
- To discuss the nature of the phase-difference polarization filter as applied to near-field and teleseismic data.

This report is organized as follows. Section II presents a description of each signal extraction technique as well as the driving module

(the three-component adaptive processor) which is common to all the signal extraction techniques discussed in this report. Section III presents the results of the work performed toward achieving the above described goals. Section IV gives the conclusions reached in the course of this work and recommendations for future work based on the evaluation of each signal extraction technique. Finally, Section V lists the references cited by this report.

SECTION II METHODOLOGY

A. THE GENERALIZED APPROACH TO SIGNAL EXTRACTION

In his report on long-period surface wave extraction, Lane (1977b) described the method of cascading signal extraction techniques to achieve greater signal-to-noise ratio gains than would be achieved by application of the techniques separately. The techniques used were Wiener filters, bandpass filters, the three-component surface wave adaptive processor, and pre-whitened matched filters. In brief, the results of this report are that the cascaded Wiener filter and three-component surface wave adaptive processor showed greater signal-to-noise ratio gains than would be predicted by summing their individual gains. Adding a matched filter following the three-component surface wave adaptive processor led to a reduction in gain. The bandpass filter-three-component surface wave adaptive processor combination yielded slightly higher gains at low input signal-to-noise ratios and slightly lower gains at high input signal-to-noise ratios than the Wiener filter-three-component surface wave adaptive processor cascade combination.

Due to the large improvements in signal-to-noise ratios found by cascading the long-period surface wave signal extraction techniques, all signal extraction techniques described in this report are cascaded. The particular extraction technique in each case is cascaded with a bandpass filter with one exception, where a Wiener filter is used in place of the bandpass filter.

A major point which all signal extraction techniques discussed in this report have in common is their driving module. This module is the three-component adaptive processor. In earlier reports on the subject of

signal extraction (e. g. , Shimshoni and Smith, 1964; Lane, 1973; and Strauss, 1976) the term 'three-component adaptive processor' has referred to a technique for extracting long-period surface waves from seismic noise. However, the actual three-component adaptive processing part of this technique is a separate module from that which computes and applies the filter weights. In this report, for example, two distinct extraction techniques, one dependent on particle-motion polarization and one dependent on phase-difference polarization, are described, each of which utilizes the three-component adaptive processing approach.

The generalized three-component adaptive processor divides the data into time segments which overlap by 50 percent, computes and applies filter weights to the data according to the particular filter model supplied, and sums and scales the filtered data segments. The idea underlying this processor is that by dividing the data into small segments, the data in each segment can be compared to the desired model on a frequency-by-frequency basis and then weighted according to their similarity to that model. Thus, the seismic noise in one segment, which does not resemble the signal model, can be rejected while the signal in another segment, which does resemble the model, can be passed. The filter weights are thus adapted to the data as the data changes in time. Thus, as the dominant wave in the data changes from noise to signal and back to noise, the filter weights change to isolate the signal. The use of overlapping segments smooths the data so that no abrupt changes are introduced from one segment to the next.

The utility of this approach becomes clearer when compared to a more conventional signal extraction technique such as a bandpass filter. In the case of a bandpass filter, the entire data sample is processed as a unit and the frequency components are accepted or rejected for the entire data sample. If the seismic noise and the signal have similar frequency content, no improvement in signal-to-noise ratio can be expected from the technique.

In the adaptive processor, measurements of the degree to which the component spectra of each data time segment resemble a specified model determines the spectrum of filter weights to be applied to that data segment. Thus, the filter weights adapt to the time-varying signal and noise characteristics of the data.

A third point which the different signal extraction techniques share in common is the trapezoidal filter weight scheme developed by Lane (1976). This is illustrated by Figure II-1. In each technique, an angle α is measured which implicitly represents the departure of the observed data from the model. For example, the Rayleigh wave model states that the difference in phase between the radial and vertical components of motion is 90° . Therefore, in this case, α_0 in Figure II-1 is 90° . If the measured angle α lies within some pre-set range ($-\alpha_1$ to α_1) about the model value α_0 , a filter weight of one is assigned. If α lies outside this range but within a second range ($-\alpha_2$ to $-\alpha_1$, α_1 to α_2), the filter weight is determined from a ramp function as shown in Figure II-1. All other values of α produce a filter weight of zero.

Figure II-2 illustrates the generalized processing scheme for each of the signal extraction techniques discussed in this report. In the first stage, the data are entered into the program and prepared for processing by zeroing out undesired portions of the data (such as spikes or glitches) and applying any pre-processors such as Wiener or bandpass filters. In the second stage, the data are segmented, Fourier transformed, compared to the model, weighted by the filter weights, inverse Fourier transformed, summed, and scaled. In the third stage, signal-to-noise ratios and magnitudes are computed as desired and the data are plotted. It is obvious that the only difference among the various techniques is the signal model used to determine the filter weights.

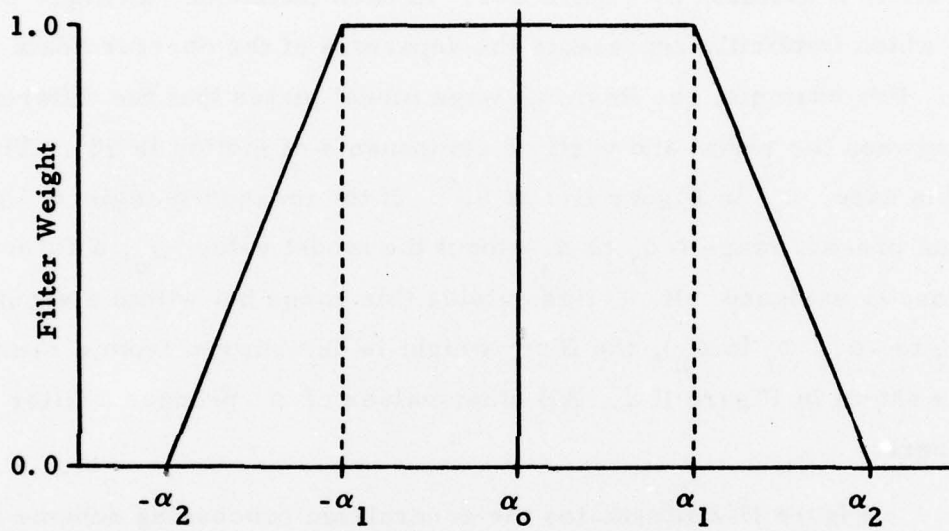


FIGURE II-1
TRAPEZOIDAL FILTER WEIGHT SCHEME

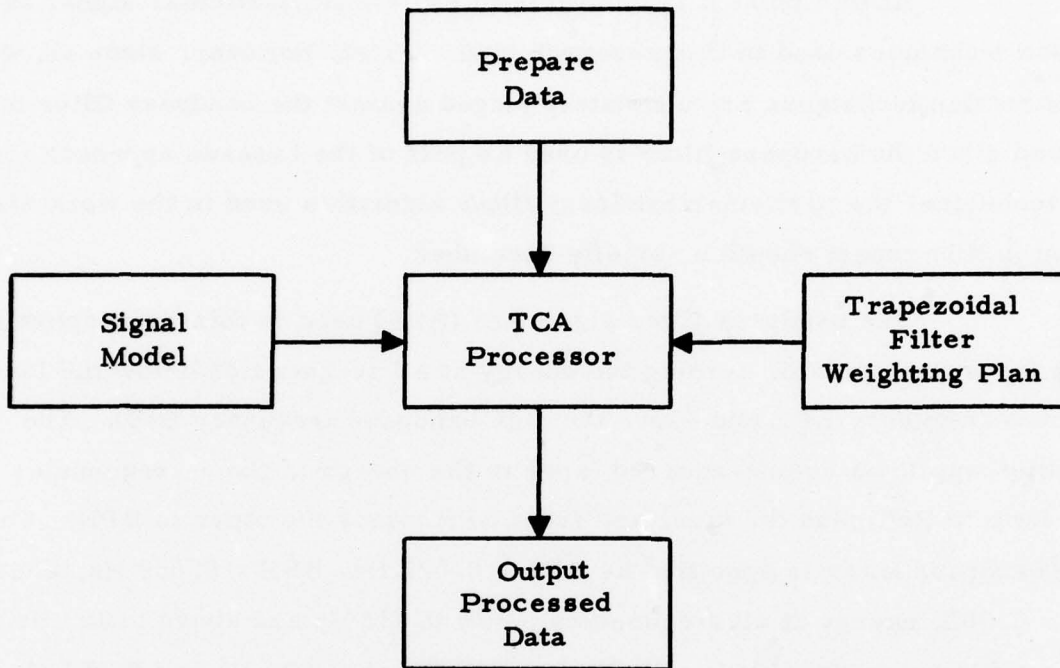


FIGURE II-2
THE GENERALIZED PROCESSING SCHEME

B. SIGNAL EXTRACTION TECHNIQUES

1. The Bandpass Filter

At this point it is desirable to review the particular signal extraction techniques used in this research task. First, however, since all signal extraction techniques are ultimately judged against the bandpass filter output, and since the bandpass filter is used as part of the cascade approach for each technique, the particular bandpass filter algorithm used in the work discussed in this report should be briefly described.

The bandpass filter algorithm (BPF) used in this work operates in the frequency domain, zeroing the energy at all frequencies below the low bandpass frequency BPL and above the high bandpass frequency BPH. The algorithm applies a cosine-squared taper to the energy at those frequencies from BPL to BPL plus the taper and from BPH minus the taper to BPH. Thus, if the bandpass filter is specified as BPL = 0.022 Hz, BPH = 0.059 Hz, and TAPER = 0.002, energy at all frequencies below 0.022 Hz and above 0.059 Hz receives a filter weight of zero and all energy between 0.024 Hz and 0.057 Hz receives a filter weight of one. The energy at the remaining frequencies receives a filter weight derived from the cosine-squared taper function.

2. The Wiener Filter

The Wiener filter (WF) is used in the study of long-period surface wave extraction. The theory underlying the design and application of Wiener filters has been discussed by Lane (1976) in some detail and will accordingly be only briefly reviewed here. The Wiener filter is one whose output is closest to the desired signal in the least mean square sense. In the frequency domain, it takes the form

$$W(\omega) = \frac{\phi_{ss}(\omega)}{\phi_{ss}(\omega) + \phi_{nn}(\omega) + \phi_{sn}(\omega) + \phi_{ns}(\omega)} \quad (\text{II-1})$$

where $\phi_{ss}(\omega)$ and $\phi_{nn}(\omega)$ are the autopower spectra of the signal and noise respectively, and $\phi_{sn}(\omega)$ and $\phi_{ns}(\omega)$ are the crosspower spectra of the signal and noise (Robinson and Treitel, 1967). The utility of this filter is that it can be used when signal and noise are only approximately known.

In designing a Wiener filter, it is necessary to estimate the terms in this equation. The noise autopower spectrum $\phi_{nn}(\omega)$ can be found from the noise preceding the signal arrival. The noise autopower spectrum was estimated by dividing the available noise data preceding the signal arrival into 256-point segments, filling out each segment with zeros to 2048 points, and Fourier transforming each segment. At each frequency, the power was the sum of the squares of the real and imaginary parts. These powers were averaged at each frequency over all available noise segments to increase the reliability of the estimates.

The signal power spectrum $\phi_{ss}(\omega)$ was found by averaging the autopower spectra of five Kurile Islands events. Before averaging, each spectrum was normalized to unit area to eliminate the influence of magnitude differences among the five events. Note that Lane (1976) used seven Kamchatka events to compute $\phi_{ss}(\omega)$. The change to Kurile Islands events was made to permit design of a filter more representative of the test data base used in this report.

It is ordinarily assumed that signal and noise are uncorrelated so that terms of the type $\phi_{sn}(\omega)$ may be ignored. However, over the data lengths used here, there may be some apparent correlation between signal and noise due to the random nature of the noise. Attempts to calculate the signal-noise correlation terms were not successful since the phase of the noise is a random variable. Although various models of the phase of the noise were examined, none was as effective as omitting the correlation terms $\phi_{sn}(\omega)$ and $\phi_{ns}(\omega)$ entirely. The Wiener filter weights are, therefore, computed from:

$$W(\omega) = \frac{\phi_{ss}(\omega)}{\phi_{ss}(\omega) + \phi_{nn}(\omega)} \quad (\text{II-2})$$

3. The Love Wave Filter

The filter (LF) used to extract long-period and short-period Love waves (LQ and Lg, respectively) is discussed in detail in terms of design and application by Strauss (1976). In brief, the method is to track the incoming Love wave in azimuth and to pass it throughout its entire duration. This is performed in the following manner for each frequency component. First, the time origin is shifted so that the vertical component is purely real. Next, the propagation direction β of the transverse component energy relative to the radial direction is calculated. The horizontal components are then rotated by $-\beta$ about the vertical axis with the result that all Love wave motion lies on the transverse component. By setting a pass window about β , the Love wave is further enhanced by rejecting all motion with arrival azimuth outside this window. (Without this window all energy, including noise, is rotated back to the transverse component.) After each frequency component has been processed in this fashion, the time origin is shifted back. For this filter, a value of 15° was used for α_1 and α_2 .

4. The Particle-Motion Polarization Filter

The particle-motion polarization filter is designed to extract long-period and short-period bodywaves from seismic noise. The model used to construct this filter is based on the linear polarization of the P wave and the plane polarization of the S wave.

Consider a P wave approaching a station at angle of incidence I_P or an S wave approaching at angle of incidence I_S . If the horizontal components are rotated so that one (the radial) points along the great circle path of the event and the second (the transverse) is perpendicular to this path

the P and S_V waves will be resolved into vertical and radial components of motion. The filter designs weights for extracting bodywave motion by first forming a unit vector \vec{U}_I in the direction of propagation using the angle of incidence. This unit vector is:

$$\vec{U}_I = \vec{U}_V \cos I + \vec{U}_R \sin I \quad (\text{II-3})$$

where the subscripts V and R denote vertical and radial motion and I represents I_P or I_S as appropriate. Next, a unit vector in the propagation direction defined by the actual recorded particle motion at each frequency is formed:

$$\vec{U}_P = \frac{A_V(f)}{(A_V^2(f) + A_R^2(f))^{\frac{1}{2}}} \vec{U}_V + \frac{A_R(f)}{(A_V^2(f) + A_R^2(f))^{\frac{1}{2}}} \vec{U}_R \quad (\text{II-4})$$

where $A_V(f)$ and $A_R(f)$ represent the amplitude at frequency f on the vertical and radial components, respectively.

Finally, the angle θ between these unit vectors is computed and tested for the presence of linearly polarized (P) or plane polarized (S) waves. This angle is computed from

$$\cos \theta = \vec{U}_I \cdot \vec{U}_P = \frac{A_V(f) \cos I + A_R(f) \sin I}{(A_V^2(f) + A_R^2(f))^{\frac{1}{2}}} \quad (\text{II-5})$$

If $\theta = 0^\circ$, the particle motion represents P waves. If $\theta = 90^\circ$, the particle motion represents S waves.

To allow for variations from event to event in the angle of incidence due to variations in crustal structure and due to the degree of refraction occurring at the crust-mantle interface, the trapezoidal pass window of Figure II-1 was used to determine the filter weights. For this filter, a value of 10° for α_1 and α_2 as defined in Figure II-1 was used.

5. The Phase Difference Polarization Filter

In the course of carrying out this research task it became apparent that a new and potentially more useful short-period and long-period bodywave and surface wave extraction technique might be developed by means of a synthesis of the principles underlying the cascaded techniques used for surface waves and the polarization technique for bodywaves.

The lead-off point for this method is the Rayleigh wave filter used in the long-period surface wave cascaded processor which searches for 90° phase differences between the radial and vertical components of motion. Noting that the polarization of P waves produces inphase vertical and radial motion and that the polarization of the S waves produces 180° out of phase vertical and radial motion, the cascaded processor using the bandpass filter and Rayleigh wave filter can be extended to extract P or S_V waves by searching for 0° or 180° phase differences between these components of motion. In addition, one can set the filter to search for prograde elliptical motion (for example, PL) by searching for 270° phase differences between the two components of motion. (In discussing the cascaded processor approach to long-period surface wave extraction, the 90° phase difference case is referred to as the Rayleigh filter (RF).)

In practice, the approach is to pass the data through the filter four times, searching for 0° phase difference (P) on the first pass, 90° phase difference (LR) on the second pass, 180° phase difference (S_V) on the third pass, and 270° phase difference (prograde elliptical motion) on the fourth pass. This, of course, only allows for signal extraction on the vertical and radial components of motion. To extract Love waves, the previously described Love wave filter is applied on the second pass. In passes one, three, and four, the filter weights computed from and applied to the vertical and radial components are also applied to the transverse component, passing whatever energy is present on that component when the sought-for phase is found on the vertical

and radial components. For example, when S_V is passed on these components, S_H is passed on the transverse component.

Finally, it should be noted that the only significant difference in interpretation of short-period and long-period data processed by this method is that with short-period data one is searching for Lg and Rg rather than LQ and LR.

C. FINAL COMMENTS ON THE METHODOLOGY OF THE EVALUATION OF SIGNAL EXTRACTION TECHNIQUES

The most common method of evaluating a signal extraction technique is to apply it to a suite of test events and, using some objective set of detection criteria, determine the decrease in the detection threshold due to this technique. The detection criteria used in this report are:

Long-period bodywaves:

- The waveform begins within ± 20 seconds of the predicted arrival time.
- The maximum amplitude of the waveform is at least twice as large as the peak amplitudes in the preceding 400 seconds of data.

Long-period surface waves:

- The waveform begins within ± 180 seconds of the predicted arrival time.
- Normal dispersion is present in the signal gate.
- The maximum amplitude of the waveform is 3 dB or more above the peak amplitudes outside the wavetrain and inside a time gate beginning 200 seconds before the predicted LQ arrival time and ending 200 seconds after the estimated LR wave end time.

- Detection of the event on at least two components of motion.

Short-period bodywaves and surface waves:

- The waveform begins within ± 5 seconds of the predicted arrival time.
- The maximum amplitude of the waveform is at least twice as large as the peak amplitudes in the preceding 40 seconds of data.

Short-period surface waves:

- Lg and Rg appear in the appropriate time windows.

During the course of processing events using the signal extraction techniques, two further points were noted which aid the analyst in making detection/non-detection decisions. First it was observed that low signal-to-noise ratio long-period surface waves lose much of their dispersive characteristics when processed by the cascade technique, but that the resultant waveforms show a highly characteristic 'packet' of energy with periods of about 20 seconds late in the signal gate. Second, the onset of short-period near-field signals commonly can be identified by an abrupt change in frequency.

The last item to be mentioned before proceeding to the results of this study is that to assess the value of any signal extraction technique, two points must be considered - signal detectability and signal measurability. If a signal extraction technique is to be useful, it must permit the analyst, using some set of detection criteria such as described above, to declare significantly more events to be detected than would be the case without use of the technique. Most commonly, comparison is made between the 50 percent detection threshold after application of the extraction technique and the 50 percent detection threshold after application of a bandpass filter. (The 50 percent detection threshold is determined by finding the number of detections and non-detections

at each m_b for a sample event population and fitting a curve to the resulting detection percentages using a maximum likelihood procedure as described by Ringdal (1974).)

A signal extraction technique may significantly lower the 50 percent detection threshold and still be of limited value if the magnitudes measured from the processed waveforms are not consistent. Any signal extraction technique can be expected to lower signal amplitudes to some extent. This is acceptable as long as two conditions are met - first, the noise must be suppressed more than the signal and second, the amount of signal suppression must be consistent from event to event. The significance of this measurability concept may best be illustrated in the context of earthquake/explosion discrimination. In the $M_s - m_b$ discriminant events can be classed as earthquakes or explosions on the basis of the difference between the m_b and M_s measured for each event. If the amount of signal suppression is known, the magnitudes measured on the waveforms can be corrected for this signal suppression. However, if the amount of signal suppression fluctuates significantly from event to event, it is quite possible that an event will be mis-classified, since any set correction factor may be too large or too small for the amount of signal suppression occurring when that particular event was processed.

SECTION III DATA ANALYSIS

A. EXTRACTION OF LONG-PERIOD SURFACE WAVES BY CASCADED PROCESSORS

The signal extraction techniques which were used in the cascaded approach to improve detectability of long-period surface waves are the band-pass filter (BPF) cascaded with the three-component surface wave adaptive processor (TCSWA) and the Wiener filter (WF) cascaded with the three-component surface wave adaptive processor as described in Section II. (The three-component surface wave adaptive processor utilizes the Love and Rayleigh filters described in Section II.) The pre-whitened matched filter used by Lane (1977b) was not used in this study, since Lane found that inclusion of this filter decreased the net signal-to-noise ratio gain of the cascaded processors. A total of 179 Kurile Islands-Kamchatka events as recorded at the Guam Seismic Research Observatory were processed by these cascaded processors.

Figure III-1 shows sample outputs from the cascaded processors for a low signal-to-noise event and a high signal-to-noise event. The data shown in Figure III-1 indicate that the portion of the Rayleigh wave best extracted by the cascaded processors is the 20-second energy. This may appear in the approximate center or toward the end of the signal gate depending on the branch of the dispersion curve or the degree of multipathing present in each test event. This 20-second energy is so characteristic of the cascaded processor output that it was included in the detection criteria. Figure III-1 also shows that in both the BPF-TCSWA and WF-TCSWA output for the low signal-to-noise event, the amount of observable dispersion is quite small, being almost nonexistent in the WF-TCSWA case. Thus, when determining whether a particular test event is detectable

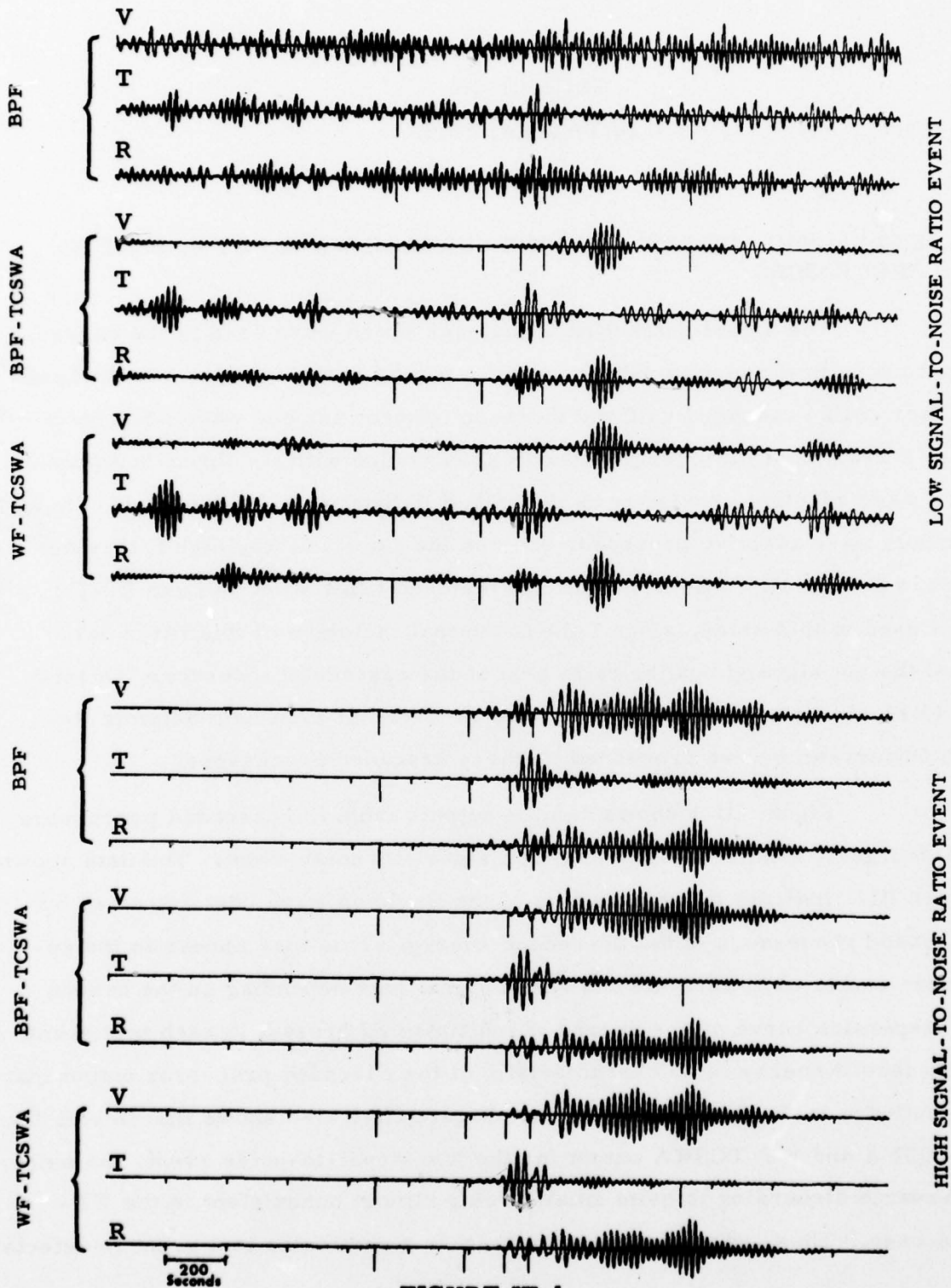


FIGURE III-1

TYPICAL DATA OUTPUT BY CASCADED PROCESSORS

after processing, the presence of the 20-second Rayleigh waveform in the signal gate becomes much more important than the presence of dispersion. As a further consequence of this lack of observable dispersion, it is advisable to measure all surface wave magnitudes at 20-second periods.

The detection statistics compiled from the 179 processed events are shown in Figure III-2. The upper portion of each sub-figure shows the number of detected and non-detected events at each m_b increment. The lower portion shows the percentage of detections at each m_b increment and the detection probability curve (solid line) and confidence limits (dashed lines) fit to these detection percentages by the maximum likelihood procedure described by Ringdal (1974). Figure III-2a shows the detection statistics derived from the bandpass filtered data. Figure III-2b shows the detection statistics derived from the data processed by the BPF-TCSWA cascaded processor, while Figure III-2c shows the detection statistics derived from the data processed by the WF-TCSWA cascaded processor. Finally, Figure III-2d shows the detection statistics for the case where an event is declared detected when the event is detected on the output of either the BPF-TCSWA or the WF-TCSWA cascaded processor.

The detection statistics are summarized in Table III-1, where the terms ' m_{b50} ' and ' m_{b90} ' refer to the 50 percent and 90 percent bodywave magnitude detection thresholds respectively. The data in Table III-1 show that use of either cascaded processor lowers the 50 percent detection threshold by approximately 0.5 m_b units. Combining the detection statistics as shown in Figure III-2d results in a decrease in the 50 percent detection threshold of approximately 0.6 m_b units. While these estimates in detection capability improvement are lower than those reported by Lane (1977b), it is felt that these new estimates are more accurate, since the test event population available to Lane did not contain sufficient non-detections at the lower m_b values to permit a good maximum likelihood fit to the detection statistics.

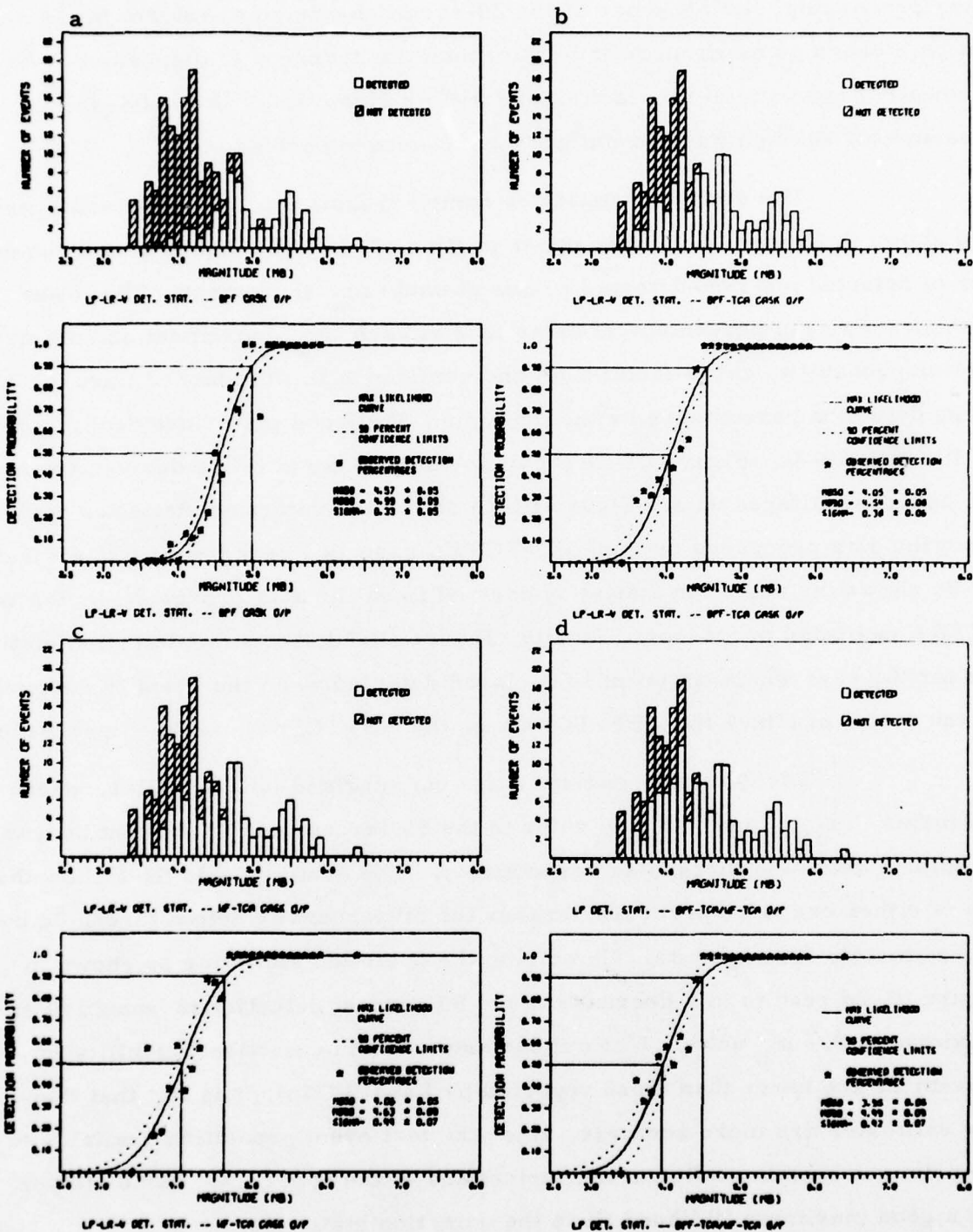


FIGURE III-2
SURFACE WAVE EXTRACTION DETECTION STATISTICS

TABLE III-1
SUMMARY OF SURFACE WAVE DETECTION STATISTICS

Processing Method	m_{b50}	m_{b90}
BPF	4.57	4.99
BPF-TCSWA	4.05	4.54
WF-TCSWA	4.06	4.63
BPF-TCSWA or WF-TCSWA	3.95	4.49

At this point, it is necessary to consider the question of measurability of the data after application of the cascaded processors. Surface wave magnitudes (M_s) were measured at 20-second periods for each test event using the automatic procedures described in the report on the evaluation of the Seismic Research Observatories (Strauss and Weltman, 1977). If the test event after processing was declared to be a non-detection, the measured M_s was called a 'noise magnitude', representing an upper bound on the actual surface wave magnitude of that event. These surface wave magnitudes were measured for each event of the data base after processing by BPF, BPF-TCSWA, and WF-TCSWA.

The purpose behind measuring noise magnitudes is to allow for the removal of positive magnitude bias from the surface wave magnitudes as detailed by Ringdal (1975) and Strauss (1978). Briefly stated, positive magnitude bias results from the normal distribution of surface wave magnitudes measured on events with a common bodywave magnitude. As this bodywave magnitude decreases, the magnitudes of the detected surface waves tend to lie on the high side of the normal distribution. Averaging the surface wave magnitudes for the detected events produces a positively biased surface wave magnitude for that bodywave magnitude, where the amount of bias increases as the surface wave detection threshold is approached.

Figures III-3 (for BPF data), III-4 (for BPF-TCSWA data), and III-5 (for WF-TCSWA data) present the measured surface wave magnitudes in terms of M_s - m_b plots. In Figures III-3a, III-4a and III-5a, the plot presents mean signal M_s versus m_b while in Figures III-3b, III-4b and III-5b the plot presents mean bias-corrected M_s versus m_b . The vertical lines through the M_s - m_b points represent plus and minus one standard deviation from the mean M_s value. (Those points for which there is no vertical line represent single events.)

Two linear fits were made to each set of M_s - m_b data. The first fit was made from the 25 percent detection threshold to $m_b = 5.0$ (the

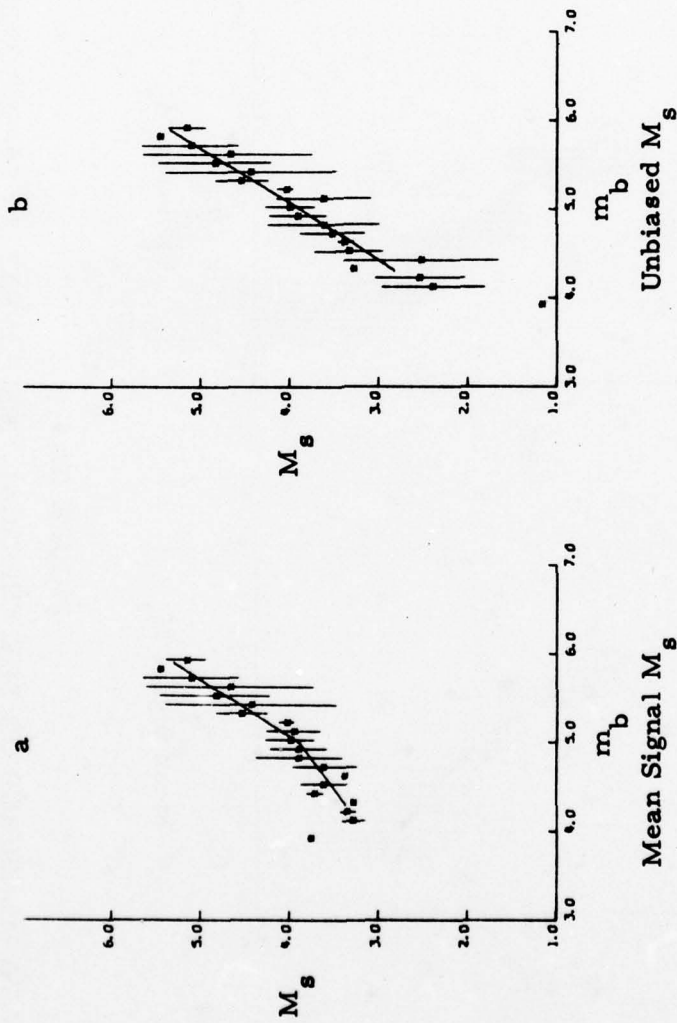


FIGURE III-3

$M_s - m_b$ DATA MEASURED ON THE VERTICAL COMPONENT AT 20-SECONDS PERIOD
AFTER BANDPASS FILTERING

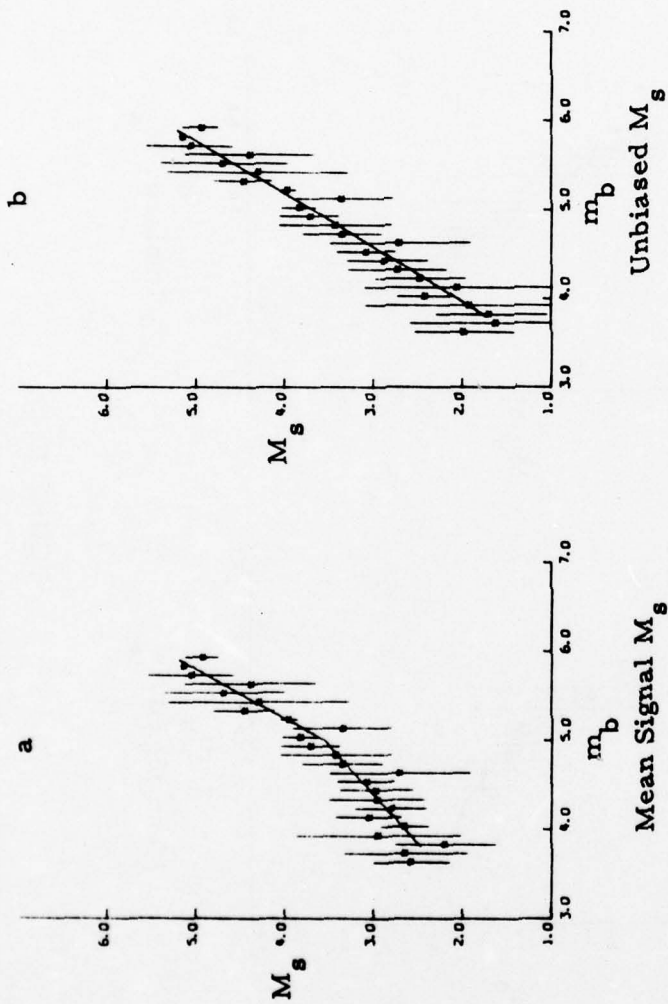


FIGURE III-4
 $M_s - m_b$ DATA MEASURED ON THE VERTICAL COMPONENT AT 20-SECONDS PERIOD
 AFTER BPF-TCSWA CASCADED PROCESSING

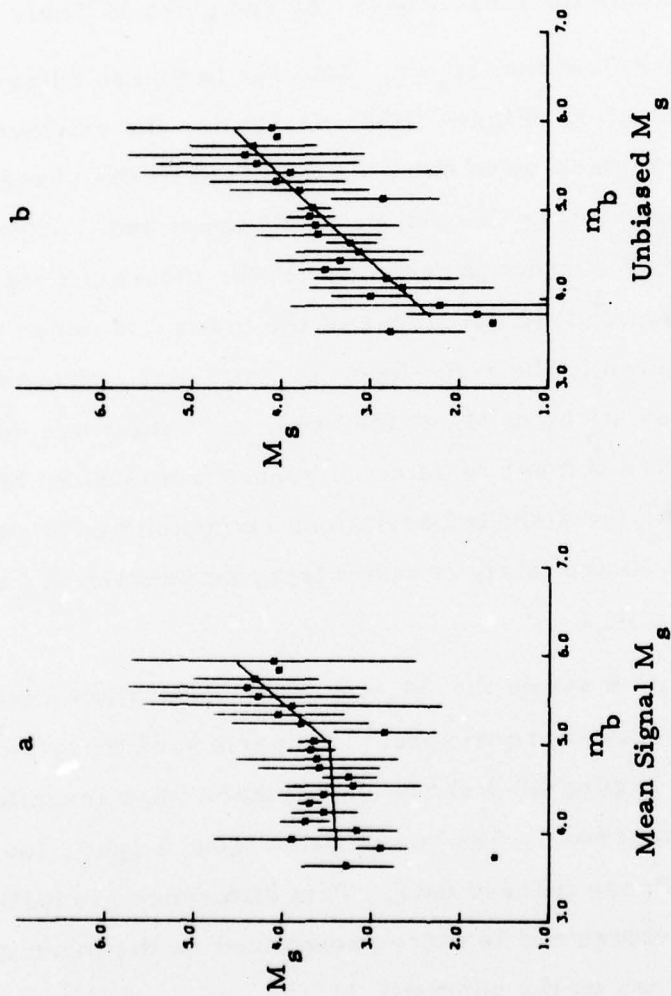


FIGURE III-5
 $M_s - m_b$ DATA MEASURED ON THE VERTICAL COMPONENT AT 20-SECONDS PERIOD
 AFTER WF-TCSWA CASCADED PROCESSING

90 percent detection threshold of the bandpass filtered data). The second fit was made from $m_b = 5.0$ to the largest m_b value of the test event population. The purpose in making two fits was to illustrate the existence of positive bias in the surface wave magnitudes at the lower m_b values. These fits were required to tie at $m_b = 5.0$. In computing these fits, each point in Figures III-3 through III-5 was weighted by the number of M_s values used to compute the mean M_s . The equations for these linear fits are given in Table III-2.

Consider first the $M_s - m_b$ data for bandpass filtered waveforms as presented in Figure III-3. Figure III-3a illustrates the existence of positive magnitude bias in the surface wave data, as indicated by the change in slope of the lower leg of the $M_s - m_b$ linear fit relative to the upper leg. After applying Ringdal's magnitude bias correction technique to the measured signal and noise surface wave magnitudes, the slopes of the lower and upper legs become nearly identical, as shown in the right-hand $M_s - m_b$ plot. Note that in Figure III-3a, the standard deviations of M_s at the lower m_b values are quite small. This is due to the limited number of detected events from which M_s could be measured. In contrast, the standard deviations computed by Ringdal's technique as shown in Figure III-3b are fairly constant (varying between 0.4 and 0.6) throughout the range of m_b .

Figure III-4 shows the $M_s - m_b$ data for surface waves processed by the BPF-TCSWA cascaded processors. Comparison of these plots with the corresponding plots of Figure III-3 shows that surface wave magnitudes measured on waveforms processed by this combination trend slightly lower than those measured on bandpass filtered data. This difference gradually increases toward the lower m_b values and is more pronounced on the mean signal (biased) $M_s - m_b$ plot than on the unbiased $M_s - m_b$ plot. Although the standard deviations are slightly larger for this data than for the bandpass filtered data of Figure III-3, it appears that surface wave magnitudes measured on data processed by this cascaded processor can be used (after addition of a bodywave

TABLE III-2
 $M_s - m_b$ RELATIONSHIPS FOR DATA OF FIGURES III-3 THROUGH III-5

PROCESSING METHOD	MEAN SIGNAL M_s				UNBIASED M_s			
	LOWER LEG		UPPPER LEG		LOWER LEG		UPPER LEG	
	FIT	S. D.						
BPF	$M_s = 0.76 m_b + 0.10$	0.32	$M_s = 1.56 m_b - 3.89$	0.56	$M_s = 1.50 m_b - 3.64$	0.42	$M_s = 1.64 m_b - 4.29$	0.57
BPF-TCSWA	$M_s = 0.91 m_b - 0.99$	0.49	$M_s = 1.81 m_b - 5.49$	0.58	$M_s = 1.62 m_b - 4.39$	0.60	$M_s = 1.69 m_b - 4.76$	0.58
WF-TCSWA	$M_s = 0.07 m_b + 3.13$	0.57	$M_s = 1.16 m_b - 2.34$	1.00	$M_s = 1.10 m_b - 1.84$	0.77	$M_s = 0.99 m_b - 1.30$	1.00

magnitude-dependent correction factor) to supplement surface wave magnitudes measured on bandpass filtered data for events not detected on the bandpass filtered data.

Figure III-5 shows the $M_s - m_b$ data for surface waves processed by the WF-TCSWA cascaded processors. These data present quite a different picture than do the data in Figures III-3 and III-4. Below $m_b = 5.0$ in Figure III-5a, the $M_s - m_b$ data have a slope near zero. After correction for magnitude bias, the slopes of the fitted $M_s - m_b$ relationships are much lower than those of the corresponding plots in Figures III-3 and III-4. This fact, coupled with the much larger standard deviations associated with the mean M_s values measured on the WF-TCSWA processed data, indicate that surface wave magnitudes measured on the output of this cascaded processor are not comparable to those measured on bandpass filtered data.

The cause of this lack of measurability must lie in the nature of the Wiener filter. There are two factors which contribute to this problem. First, the Wiener filter requires a model of the signal in order to compute the signal auto-power spectrum $\phi_{ss}(\omega)$. As mentioned in Section II, this model is an average of five Kamchatka signals. However, the Kurile Islands-Kamchatka events show large variations in the character of their surface waves caused by source and path variations. Any one model, therefore, cannot be expected to closely represent all of these events. When the model is close to the test waveform, a relatively high M_s value will be measured. As the model departs from the character of the test waveform, relatively lower M_s values will be measured. This would tend to increase the variance in the M_s measurements for a given m_b . The second factor which contributes to this measurability problem is that the Wiener filter uses the noise data recorded just prior to the signal arrival to compute the noise auto-power spectrum $\phi_{nn}(\omega)$ required by equation II-2. It is possible that this noise gate actually contains small undetected signals, raising the value of $\phi_{nn}(\omega)$. This would result in the application of

erroneously small filter weights to the data, decreasing the measured surface wave magnitudes.

With these points in mind, it is surprising not that the data processed by the WF-TCSWA cascaded processor lacks measurability but that it increases the detectability of the data as much as it does. The implication of this is that Wiener filters designed for application to events with less complex source regions and travel paths might be quite useful in extending the detectability and measurability of long-period surface wave data.

B. EXTRACTION OF LONG-PERIOD BODYWAVES BY PARTICLE-MOTION POLARIZATION FILTERS

This portion of the report examines three points related to the extraction of bodywaves from seismic noise. First, the reason for the poor performance of the particle-motion polarization filters when applied to long-period Kurile Islands-Kamchatka events as recorded at the Guam Seismic Research Observatory (Lane, 1977a) must be examined. Second, it is necessary to determine whether these filters will perform better when applied to a different long-period data base. Finally, it is necessary to determine whether it is feasible to apply these filters to near-field short-period data.

Lane (1977a) reported that particle-motion polarization filters when applied to long-period Kurile Islands-Kamchatka bodywaves as recorded at Guam produced essentially no decrease in the P wave detection threshold and actually raised the S wave detection threshold. Figure III-6a presents one of these events. First, one can note that on the traces marked 'S- filter', there is no apparent S wave motion following the expected S wave arrival time after application of this filter, even though a waveform at the expected arrival time of SS can be picked on the bandpass filtered traces. The absence of S on this record may be due to a null in the radiation pattern, but one would expect that if the observed waveform at the SS expected arrival time is indeed SS, it would

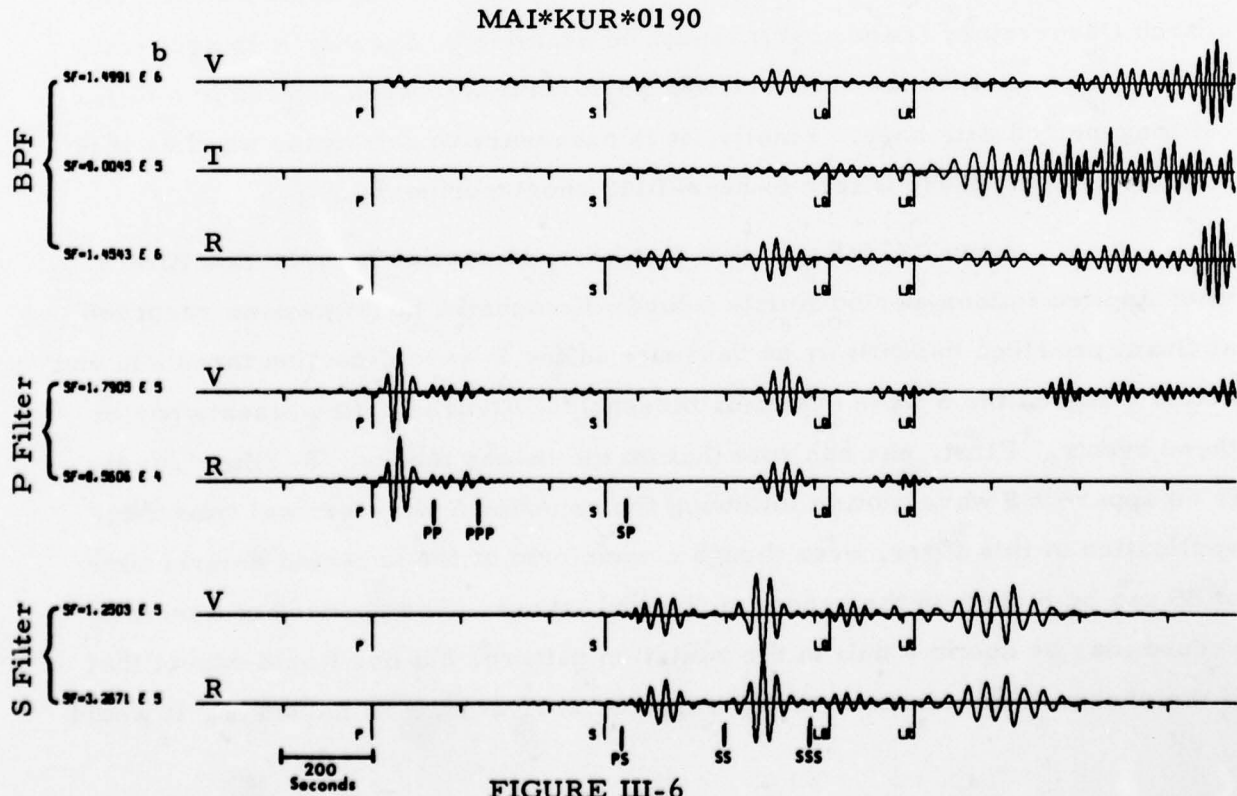
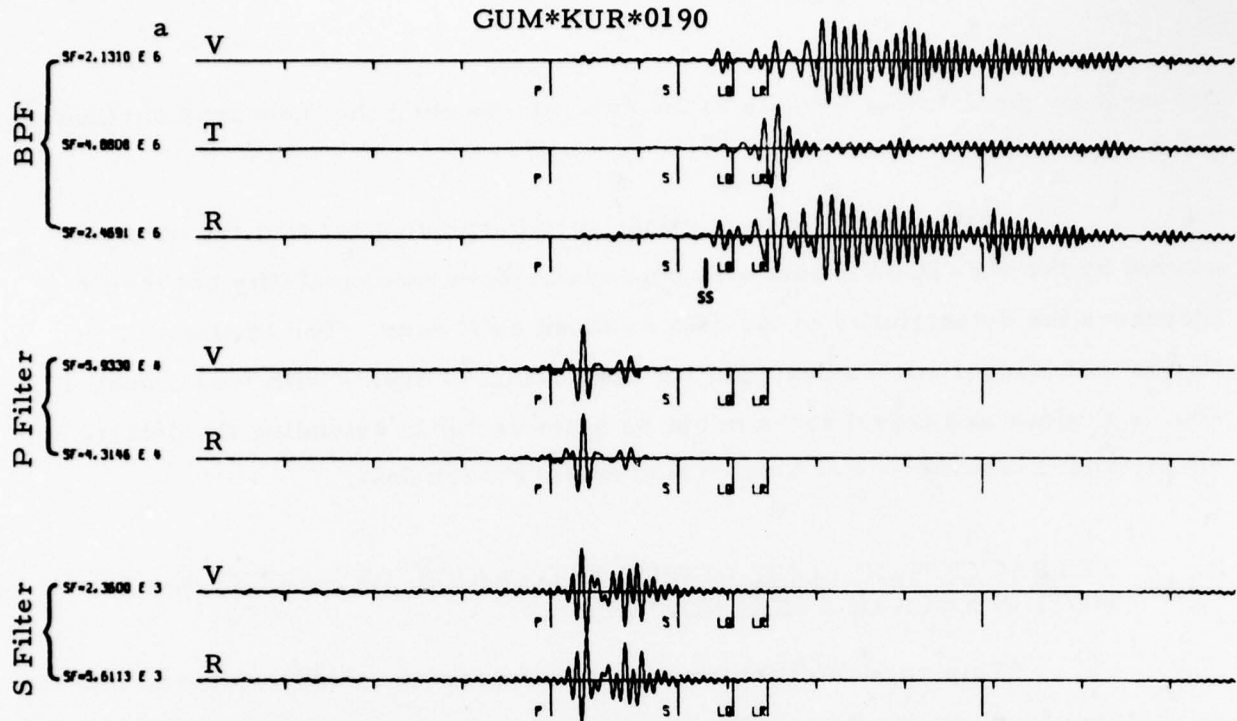


FIGURE III-6

SAMPLE OUTPUTS FROM PARTICLE-MOTION POLARIZATION FILTER

have been passed by the filter. A possible explanation for this apparent failure of the filter to pass shear waves is that the shear wave particle motion has been distorted by the surface waves which immediately follow in the record. That the filter itself is not at fault is borne out by Figure III-6b, which shows the same event as recorded at the Mashhad Seismic Research Observatory. The epicentral distance is approximately twice that at Guam, giving greater separation in time between the phases. Note that in Figure III-6b, both P and S motion appear at the appropriate time on the appropriate traces.

The lack of improvement in the P wave detectability for the Guam to Kurile Islands-Kamchatka events appears to be due to Guam lying near a null in the P wave radiation pattern. Bullen (1965) states that the more distant a point on the Earth's surface is from an initial earthquake disturbance, the more prominent are the surface waves as compared with the bodywaves. The vertical component data in Figure III-6, however, show P to LR ratios of 0.028 for the Guam-recorded data ($\Delta = 35^\circ$) and 0.119 for the Mashhad-recorded data ($\Delta = 66^\circ$). This indicates that Guam lies much closer to a null in the P wave radiation pattern than does Mashhad.

The waveform appearing on the S-filter traces at the expected P arrival time requires some explanation. Figure III-7 from Ewing, Jardetsky, and Press (1957) illustrates the origin of this shear wave energy. The P wave incident at the Moho is refracted as P and S and reflected as PP and PS. According to Richter (1958), the largest portion of the incident P wave energy is contained in the refracted P, with the remaining energy partitioned among the refracted S and the reflected PP and PS. The scale factors of Figure III-6a show that the ratio of the refracted S to refracted P is 0.04 for the vertical component and 0.13 for the radial component. Thus, the waveform seen on the S-filtered traces of Figure III-6a appears to be due to the conversion of P to S at the Moho.

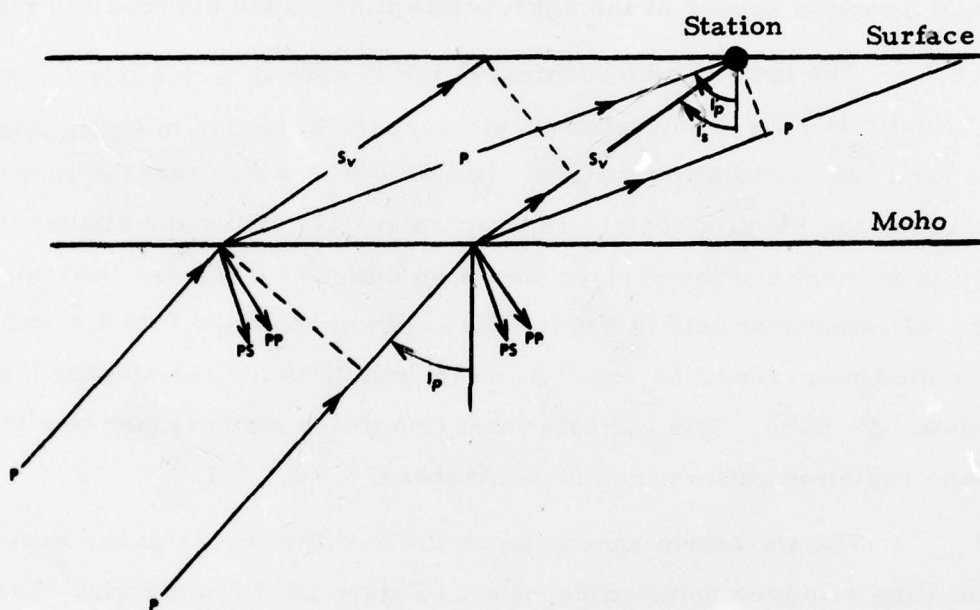
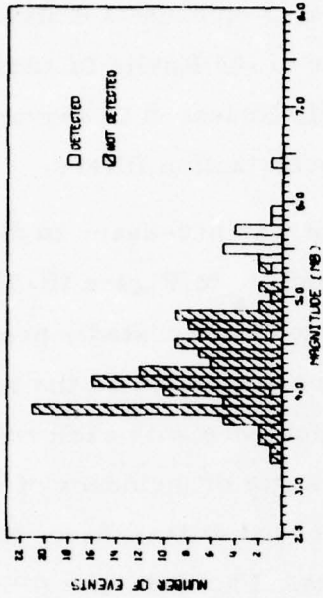


FIGURE III-7
 REFLECTION AND REFRACTION OF P WAVES AT AN INTERFACE
 BETWEEN TWO ELASTIC SOLIDS

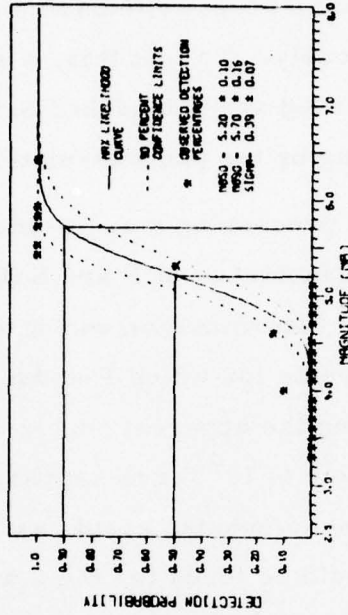
The data of Figure III-6b give hope that the particle-motion polarization filter will produce a significant improvement in bodywave detectability when applied to an event suite having greater epicentral distances than the events used previously. To test this, a suite of 144 Kurile Islands-Kamchatka events as recorded at the Mashhad Seismic Research Observatory was selected for processing by the particle-motion polarization filters.

Before processing these events, it was necessary to determine the apparent angles of incidence of P and S (I'_p and I'_s in Figure III-7) at the station. An empirical determination was attempted by repeatedly processing several large m_b events for which P and S were detectable on the bandpass filtered traces, varying the apparent angles of incidence with each run. This approach yielded a value of 19° for the apparent angle of incidence of the P wave of Kurile Islands-Kamchatka events as recorded at Mashhad. However, no clear-cut result could be found for the S waves. Pho and Behe (1972) report a value of approximately 20° for the P wave angle of incidence at this epicentral distance, while Chandra (1972) reports a value of approximately 22° for the S wave angle of incidence. Since the empirical and tabulated P wave angles of incidence agree so well, the tabulated values for both P and S angles of incidence were used to process the data base.

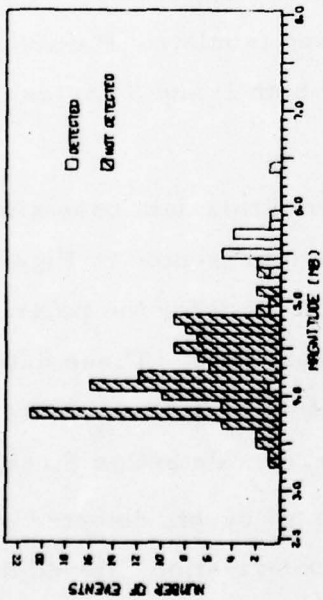
The detection statistics derived from this data base after application of the particle-motion polarization filter are presented in Figure III-8 for the bandpass filtered bodywave data and Figure III-9 for the polarization filtered data. The results are summarized in Table III-3. These detection statistics indicate detection capability improvements of 0.3 m_b units for P waves and 0.4 m_b units for S waves at the 50 percent detection threshold due to application of these polarization filters. Since all events detected on the bandpass filtered data were also detected on the polarization filtered data, the increase in the 90 percent detection threshold for the P wave data must be an artifact of the data base which causes an increased uncertainty in defining the



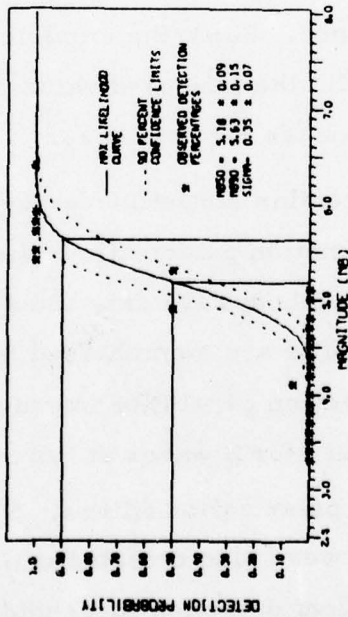
LP-5 DET. STAT. -- BPF DATA -- M₀10



LP-5 DET. STAT. -- BPF DATA -- M₀10



LP-4 DET. STAT. -- BPF DATA -- M₀10



LP-4 DET. STAT. -- BPF DATA -- M₀10

FIGURE III-8

DETECTION STATISTICS MEASURED ON BANDPASS FILTERED BODY WAVES -
MASHHAD-KURILE ISLANDS, KAMCHATKA DATA BASE

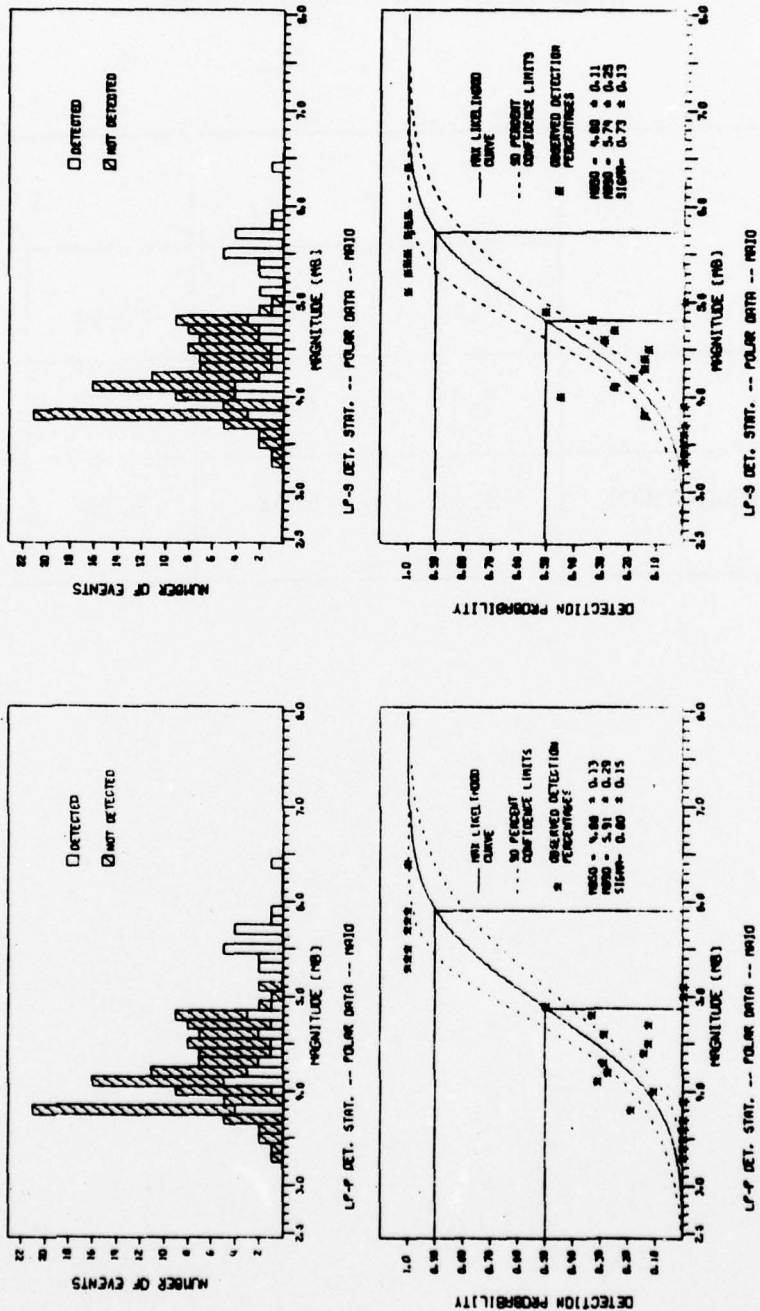


FIGURE III-9
 DETECTION STATISTICS MEASURED ON PARTICLE-MOTION POLARIZATION FILTERED BODY WAVES -
 MASHHAD-KURILE ISLANDS, KAMCHATKA DATA BASE

TABLE III-3
COMPARISON OF BANDPASS FILTER AND PARTICLE-MOTION POLARIZATION
FILTER DETECTION THRESHOLDS FOR LONG-PERIOD
MASHHAD-RECORDED EVENTS

	P		S	
	m_{b50}	m_{b90}	m_{b50}	m_{b90}
BPF	5.18	5.63	5.20	5.70
POLARIZATION	4.88	5.92	4.80	5.74

detection curve. Note from Figures III-8 and III-9 that the data base is sparse at the higher bodywave magnitudes and that the majority of detections due to this polarization filter are at the lower bodywave magnitudes. This combination causes the 90 percent detection threshold (as computed by Ringdal's maximum likelihood method (Ringdal, 1974)) to shift to higher values. Resolution of the effect of the particle-motion polarization filter on the 90 percent detection threshold must await the gathering of a data base rich in high m_b events.

Having considered the effect on long-period bodywave detectability of the particle-motion polarization filter, it is now necessary to consider the measurability of the data after being so processed. Figure III-10 shows Mashhad-recorded P wave maximum amplitudes measured on the bandpass filtered data plotted against P wave maximum amplitudes measured on the particle-motion polarization filtered data. If this filter caused no signal attenuation relative to the bandpass filtered signal, the points would lie on the dashed line. If the amount of signal attenuation was constant, the points would form a line below and parallel to the dashed line. However, the data in this figure show that below a bandpass amplitude of 1000 (corresponding to a long-period bodywave magnitude of approximately 5.2 as determined from the P-factors of Veith and Clawson (1972)), the attenuation due to application of the polarization filter begins to increase toward lower bandpass filter amplitudes. Since the 50 percent detection threshold for long-period P waves after bandpass filtering is at $m_b = 5.2$, one can expect amplitudes measured for bodywaves detected only after polarization filtering to be significantly lower than the actual P wave amplitude of the event.

C. EXTRACTION OF SHORT-PERIOD BODYWAVES BY PARTICLE-MOTION POLARIZATION FILTERS

The feasibility of applying the particle-motion polarization filter to near-field short-period data is the next point to be considered. The one

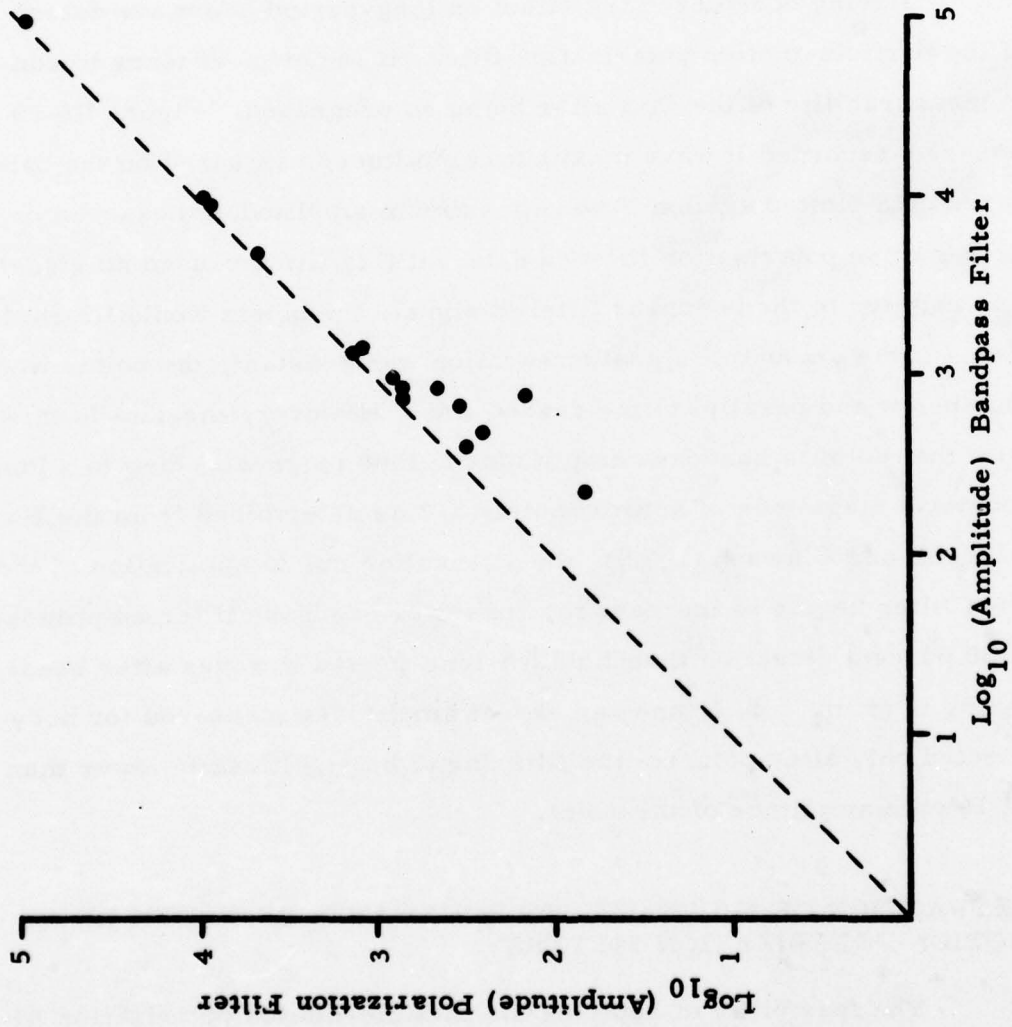


FIGURE III-10

MEASURABILITY OF P WAVES PROCESSED BY THE PARTICLE-MOTION POLARIZATION FILTER

difficulty encountered in attempting to apply these filters to near-field short-period data is the determination of angles of incidence of P and S. A search of the literature revealed very little information on this subject. The tables of P wave angles of incidence prepared by Pho and Behe (1972) and the tables of S wave angles of incidence prepared by Chandra (1972) do not include data for epicentral distances less than 20° . Papazachos (1964) discusses angles of incidence for P in the epicentral distance range 10° to 95° , presenting the data in the form of plots of angle of incidence versus epicentral distance. Mereau (1965) in a study of near-field explosion data recorded in Ontario, Canada, found P wave apparent angles of incidence of 40° to 50° for epicentral distances less than 2° and 20° to 39° for epicentral distances between 2° and 4° .

An attempt was made to empirically determine angles of incidence by making multiple runs of the short-period version of the particle-motion polarization filter program on several large bodywave magnitude events, changing the angle of incidence with each run. However, the results showed the same large variations as those reported by Mereau.

The difficulty of obtaining good estimates of angles of incidence for near-field short-period bodywaves may be explained by reference to Figure III-11, which shows the travel paths of the near-field P phases. From Figure III-11, one can see that three angles of incidence, one for each P phase, must be determined in order to apply the particle-motion polarization filters to this type of data. An analogous situation, of course, exists for the S phases S_g , S^* , and S_n .

Figure III-12 shows a sample output of the short-period particle-motion polarization filter program. Note that for the angle of incidence used, the P_g phase has been greatly enhanced relative to the P_n phase, indicating that the angle of incidence used to produce this figure is more appropriate for P_g than P_n . On the S-filtered traces, no clear start of the S phases can be picked, although the shear phases have been enhanced relative to the remainder of the data.

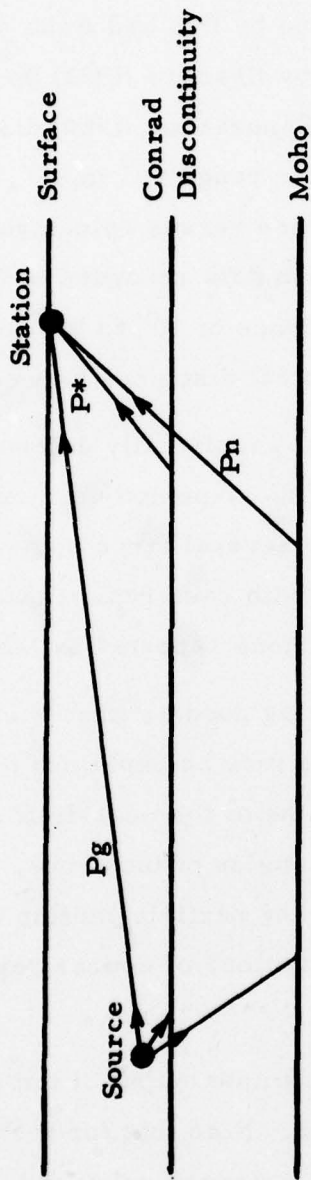


FIGURE III-11
 TRAVEL PATHS OF P_n , P^* , AND P_g (MODIFIED FROM RICHTER, 1958)

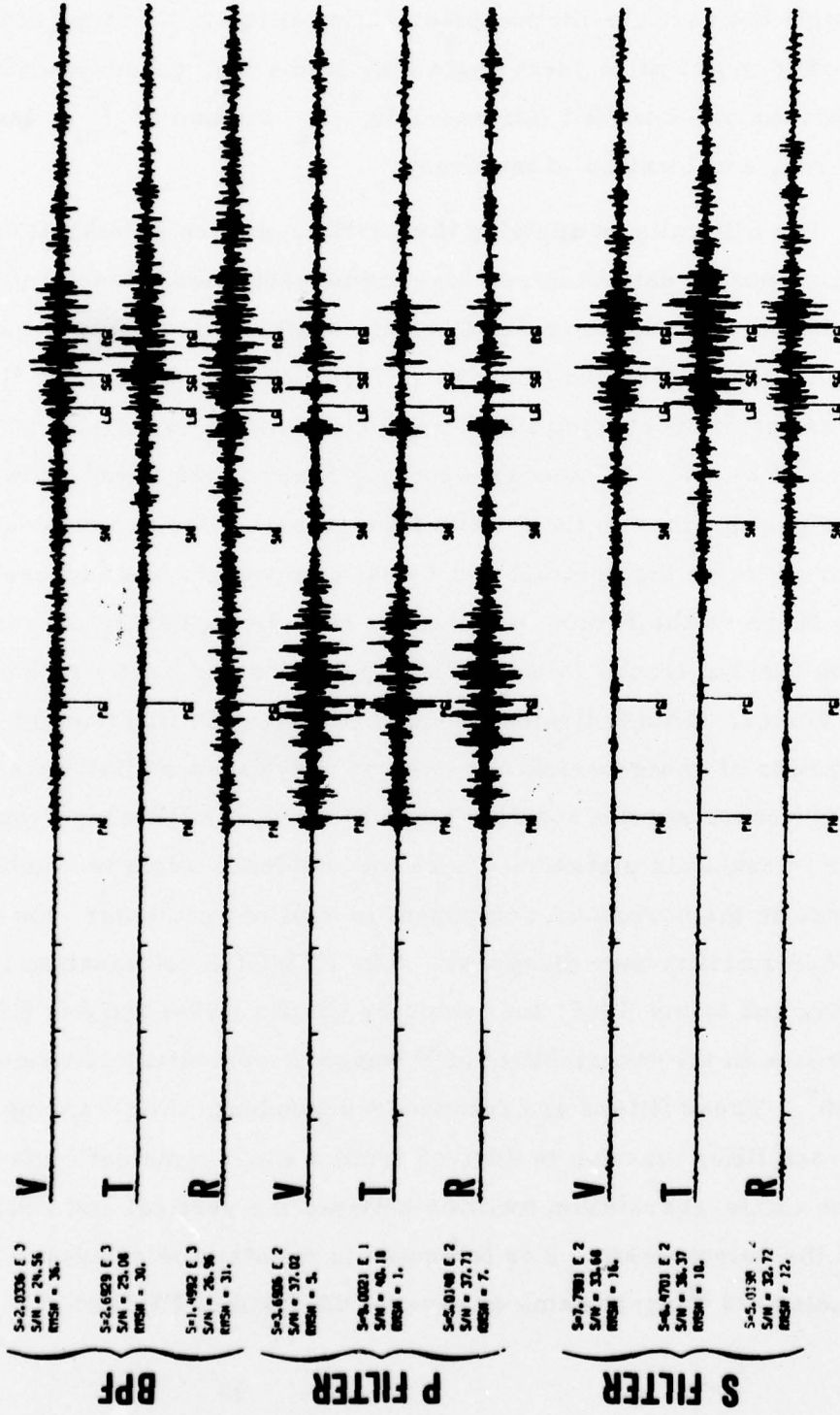


FIGURE III-12

SAMPLE OUTPUT FROM SHORT-PERIOD PARTICLE-MOTION POLARIZATION FILTER PROGRAM
 APPLIED TO A NEAR-FIELD ($\Delta = 5.84^\circ$) EVENT

In summation, it appears that unless a detailed study of the angles of incidence for short-period near-field bodywaves is made, it is not advisable to apply the particle-motion polarization filter to this type of data, since an incorrect choice of incident angle may lead to the enhancement of a phase other than the one intended (for example, P_g instead of P_n), leading to incorrect timing and location of the event.

The difficulty in applying the particle-motion polarization filter program to short-period data becomes less significant when teleseismic data ($\Delta > 20^\circ$) is to be processed, since for this data angles of incidence from the tables of Pho and Behe (1972) and Chandra (1972) can be used. Figure III-13 presents the results of processing the P wave signal of an event with an epicentral distance of 21.17° . (The corresponding S wave data is not shown, since another signal arrives in the S wave time gate.) After processing, the signal-to-noise ratio for the vertical and radial components has increased by approximately 10 dB as the P wave progresses from being barely perceptible on the bandpass filtered traces to being clearly defined and easily picked on the processed traces. This indicates that this polarization filter might be useful in the extraction of short-period teleseismic bodywaves at distances of about 20° . For weaker signals not detectable by bandpass filtering, especially at much larger teleseismic distances where the incidence angle is much smaller and the signal on the horizontal component is still much weaker, the apparent increased detectability may disappear. The REMODE polarization filters, developed by Sax and Mims (1965) and tested by Griffin (1966) and Sax (1966), showed no increase in the detectability of P waves at epicentral distances greater than 40° . These filters are frequency-dependent, time-varying filters in which each filter function is derived from a short-time estimate of the even part of the cross-correlation function between the vertical and radial components of the seismogram. For teleseismic events, the results of the application studies did suggest gains of several dB for the PP and SP phases.

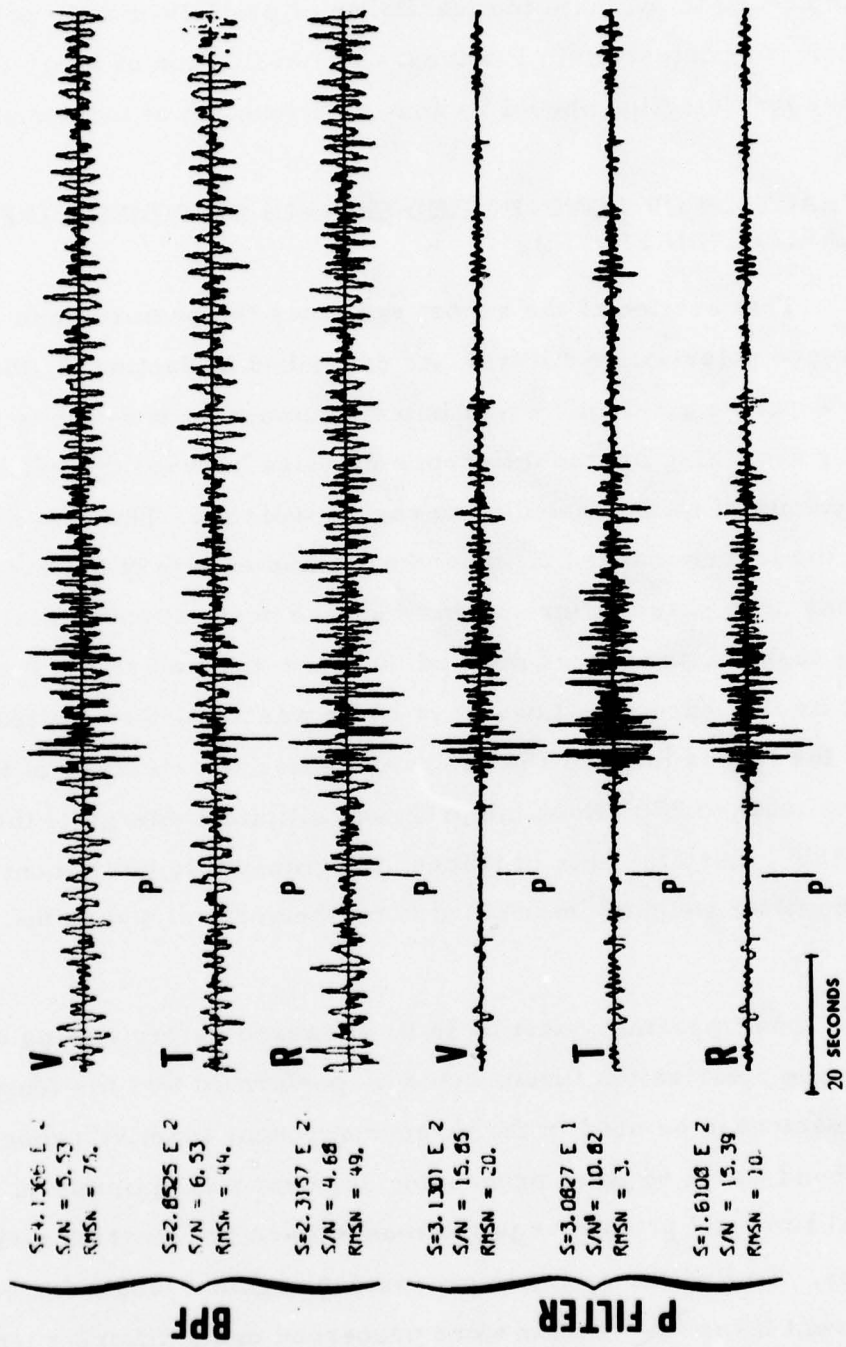


FIGURE III-13

SAMPLE OUTPUT FROM SHORT-PERIOD PARTICLE-MOTION POLARIZATION FILTER PROGRAM
 APPLIED TO A TELESEISMIC ($\Delta = 21.17^\circ$) EVENT

More data is needed to evaluate the feasibility of particle-motion polarization filters for detecting teleseismic P waves. The evaluation of short-period teleseismic bodywave detection should be done as a function of incidence angle.

D. EXTRACTION OF LONG-PERIOD SIGNALS BY PHASE-DIFFERENCE POLARIZATION FILTERS

This section of the report examines the performance of the phase-difference polarization filters. As described in Section II, these filters allow one to separate a seismic event into its component bodywaves and surface waves by searching for the difference in phase between the vertical and radial components of motion peculiar to each waveform. Thus, in the following figures, the traces marked 0° show the P wave energy of the event, since the P wave has zero phase difference between the vertical and radial components. In like fashion, the traces marked 90° show the Rayleigh wave energy of the signal (in this case, the Love wave filter was applied to the transverse component), the traces marked 180° show the shear wave energy of the signal, and the traces marked 270° show the prograde elliptical energy of the signal. For the 0° , 180° , and 270° sets of traces, the transverse component has been filtered by the filter weights determined from the vertical and radial components.

One important question to be answered before testing of the phase-difference polarization filters could be performed was the length of the processing segment to be used in the three-component adaptive processor. Lane (1976) found that a 64 point processing segment was optimum in terms of computational time and processor performance when processing dispersed surface waves. To find the optimum processing segment length for bodywaves, several different large m_b events were processed using different lengths. From this, the best processing segment length for bodywaves was found to be 32 points. Examples of this are shown in Figure III-14 for the 32 point processing segment and Figure III-15 for the 64 point processing segment. Note

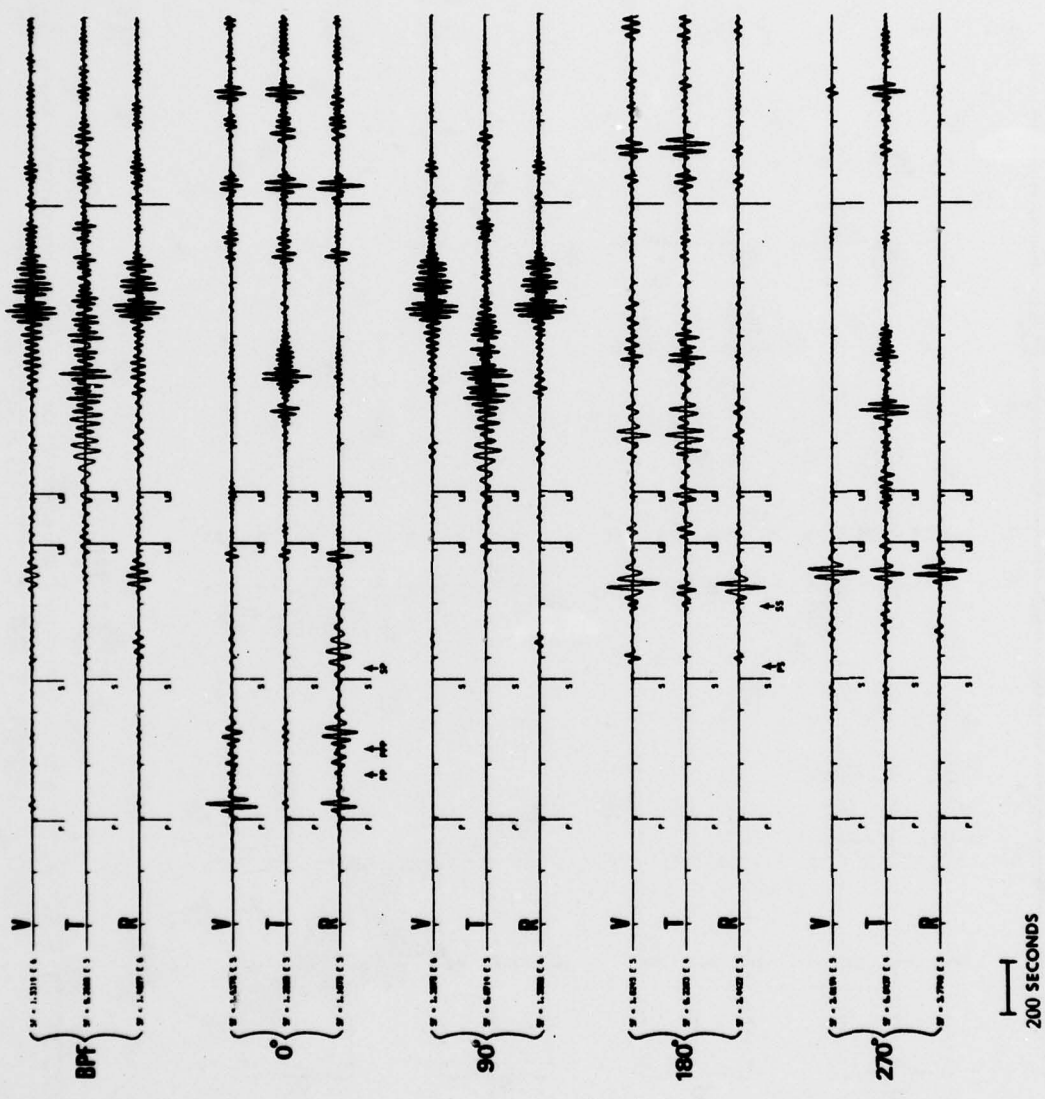


FIGURE III-14
 SAMPLE OUTPUT FROM THE PHASE-DIFFERENCE POLARIZATION FILTER PROGRAM
 USING A 32 POINT PROCESSING SEGMENT

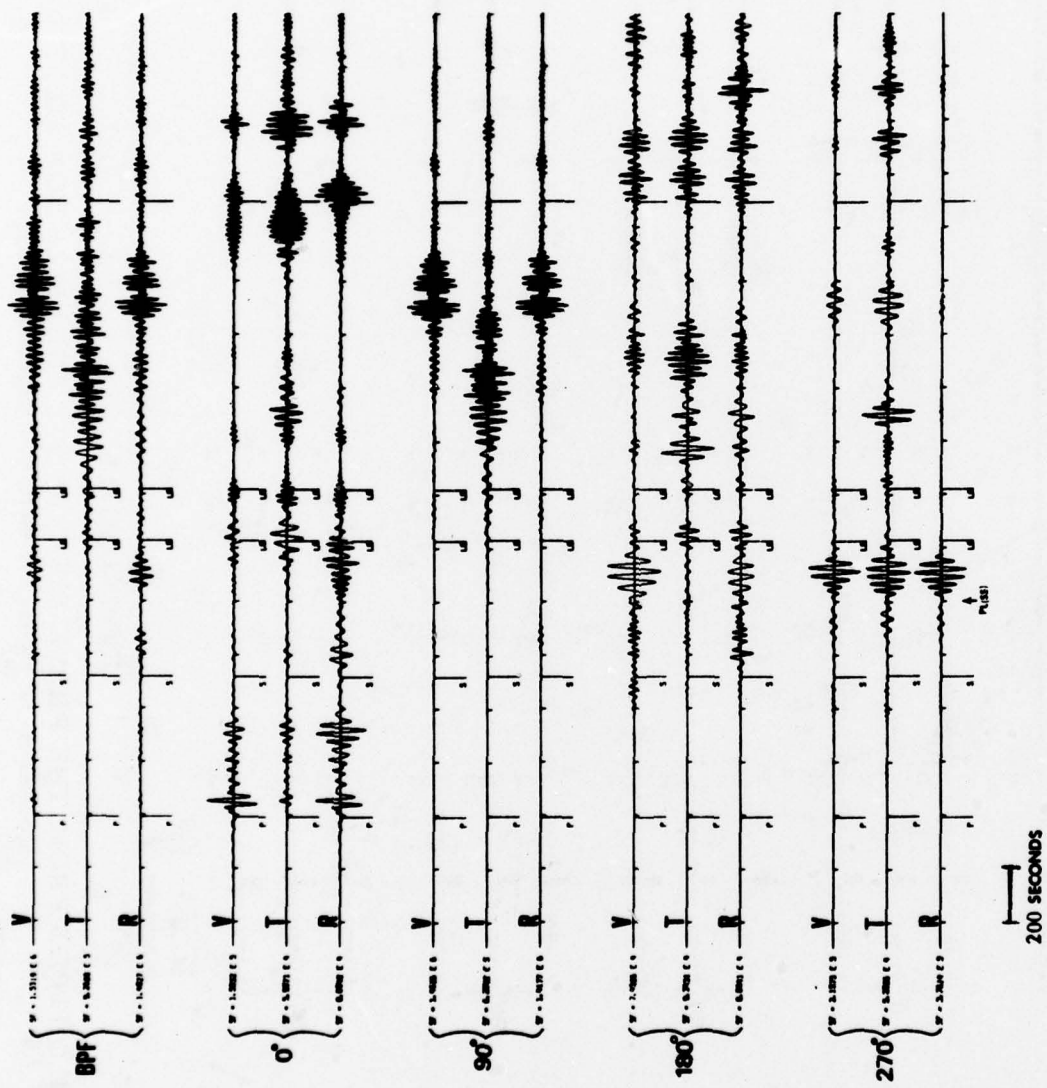


FIGURE III-15
 SAMPLE OUTPUT FROM THE PHASE-DIFFERENCE POLARIZATION FILTER PROGRAM
 USING A 64 POINT PROCESSING SEGMENT

that when a 32 point processing segment is used, the P, PP, and PPP phases can be easily picked, whereas when a 64 point processing segment is used, these phases do not clearly separate. The same situation can be seen to occur for the shear phases on the 180° traces.

The tick marks on Figures III-14 and III-15 show the predicted arrival times of the various body and surface waves as computed from the travel-time tables of Jeffreys and Bullen (1967). These figures illustrate the value of this form of filtering in the analysis of seismic signals. For example, note in Figure III-14 the enhancement of P, PP, and PPP on the traces marked 0° in comparison to the bandpass filtered traces. The apparent shear wave on the bandpass filters resolves into SP on the 0° traces and PS on the 180° traces. The waveform just preceding the LQ tick mark on the 0° traces may be SS converted to P at the Moho in the manner illustrated by Figure II-7.

The most interesting feature of Figure III-15 is the waveform designated PL(SS) on the 270° traces. PL(SS) is interpreted as a shear-coupled PL generated by the SS waveform. (The notation PL(SS) follows that of Poupinet and Wright (1972).) The PL phases PL, PL(S), and PL(SS) are in general difficult to identify, since they appear on bandpass filtered data as part of the coda of the generating waveform. Oliver (1964), for example, defines PL as the normally-dispersed prograde elliptical long-period wavetrain observed during the interval between the initial P wave and the S wave. However, identification of PL in this gate, PL(S) in the gate following the S arrival, or PL(SS) in the gate following the SS arrival is not easily made, since the reflected waveforms (i. e., PP, PPP, PS, SP, SS, and SSS) also arrive in these gates. By suppressing all waveforms which do not have the correct phase difference between the vertical and radial components of motion, it is possible to separate and identify these PL phases. Figure III-16 presents a scaled-up plot of the bodywave portion of Figures III-14 and III-15. The 0° and 180° traces were filtered using a 32 point processing segment, while the 90° and 270° traces were filtered using

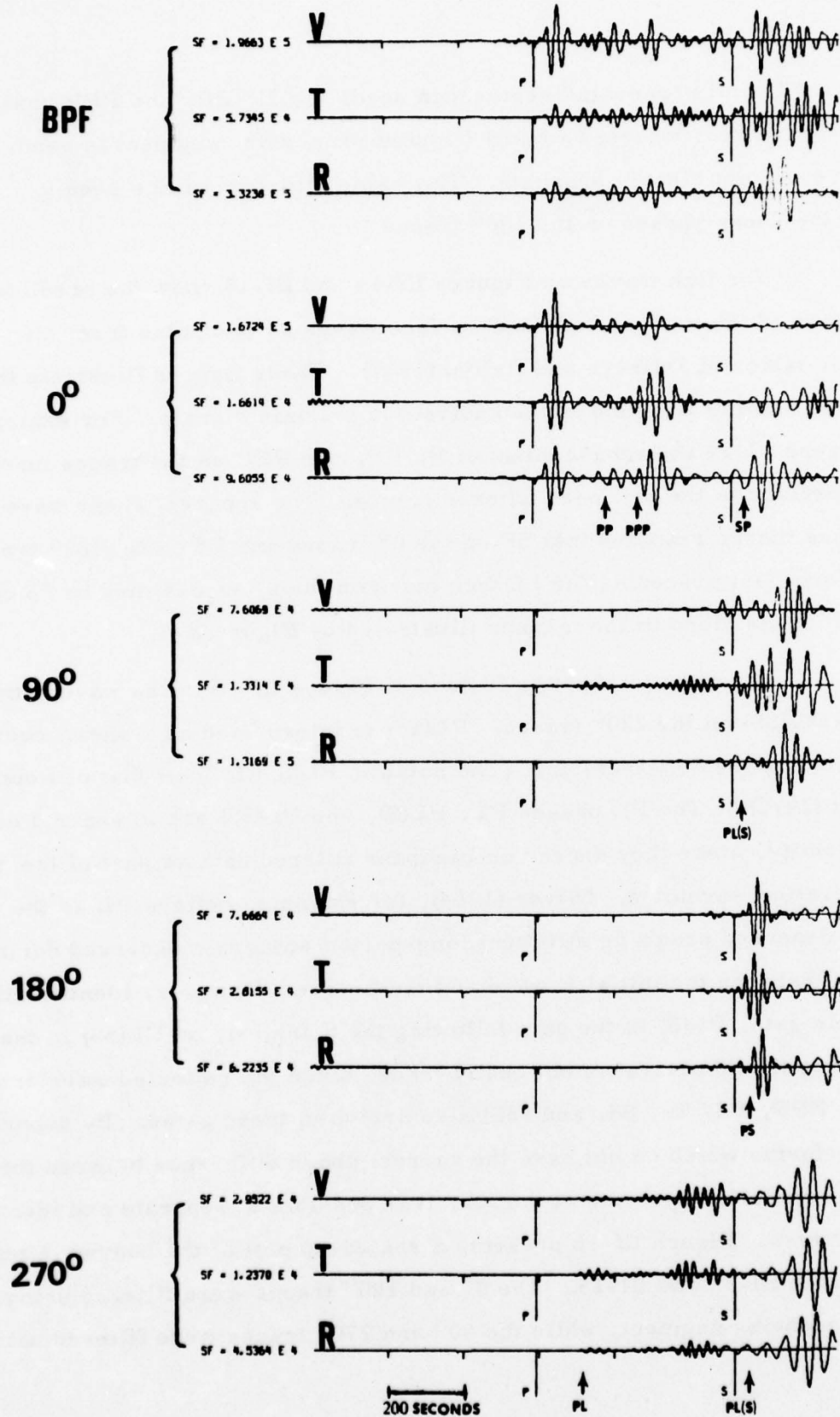


FIGURE III-16

SCALED-UP PLOT OF THE BODYWAVE DATA OF
 FIGURES III-13 AND III-14
 III-32

a 64 point processing segment. Tick marks have been added to show the expected start time of PL and PL(S). A small amplitude waveform starting at the PL tick mark can be observed on the 270° (prograde elliptical) traces. Waveforms starting at the PL(S) tick marks can be observed on both the 90° (retrograde elliptical) and 270° (prograde elliptical) traces.

The next point to consider is the improvement in detectability of seismic waves due to application of the phase-difference polarization filter. The surface wave detection threshold improvement has already been presented in Part A of this section, where it was determined that use of the bandpass filter-three-component surface wave adaptive processor lowered the 50 percent detection threshold by $0.5 m_b$ units.

With the surface wave detection threshold improvement already determined, it was not necessary to re-run all the events of the data base with this particular form of the phase-difference polarization filter. In order to save computational time while determining the detection threshold of the long-period P and S bodywaves, the program was cut down to the 0° and 180° phase-difference filters. The events of the Mashhad-Kurile Islands, Kamchatka data base were then processed and picked using the appropriate detection criteria of Section II. The resulting detection statistics are shown in Figure III-17 and summarized in Table III-4, where the 50 and 90 percent detection thresholds for bandpass filtered bodywaves are taken from Figure III-8. These results, together with the earlier-derived results for surface waves, show that the phase-difference polarization filter lowers the 50 percent detection threshold of long-period P, S, and surface waves by approximately $0.5 m_b$ units.

The last point to be considered in discussing application of the phase-difference polarization filter to long-period data is the measurability of the data after processing. (The measurability of surface waves will not be recounted here, as it is covered in Part A of this section.) Figure III-18 presents a plot of the peak P wave amplitude measured on bandpass filtered

TABLE III-4
 COMPARISON OF BANDPASS FILTER AND PHASE-DIFFERENCE POLARIZATION
 FILTER DETECTION THRESHOLDS FOR LONG-PERIOD
 MASHHAD-RECORDED EVENTS

	P		S	
	m_{b50}	m_{b90}	m_{b50}	m_{b90}
BANDPASS FILTER	5.18	5.63	5.20	5.70
POLARIZATION FILTER	4.65	5.53	4.62	5.54

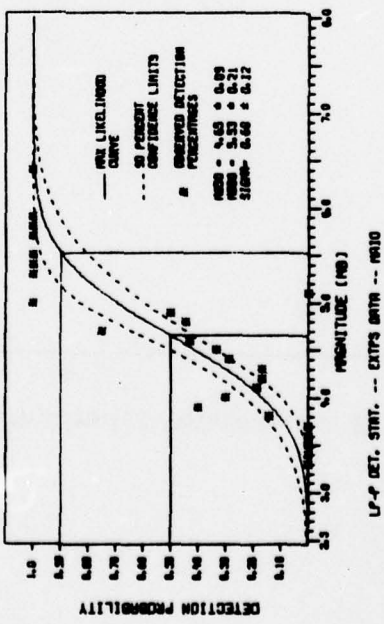
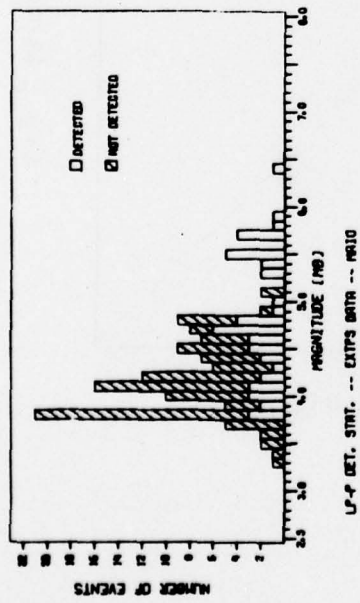
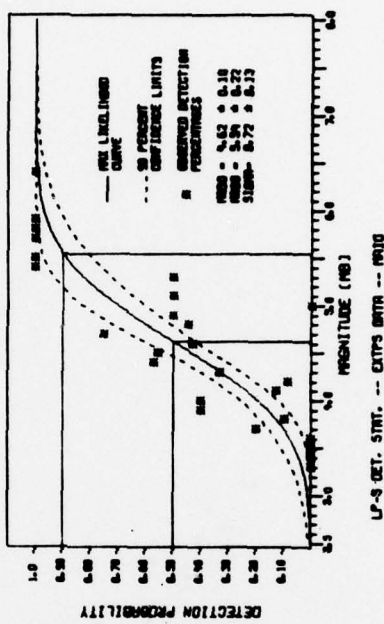
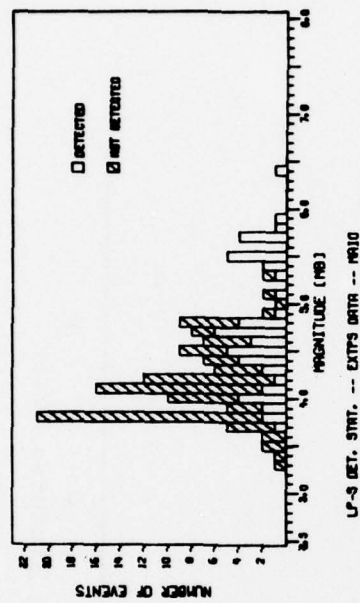


FIGURE III-17
 DETECTION STATISTICS MEASURED ON PHASE-DIFFERENCE POLARIZATION FILTERED BODY WAVES -
 MASHHAD - KURILE ISLANDS, KAMCHATKA DATA BASE

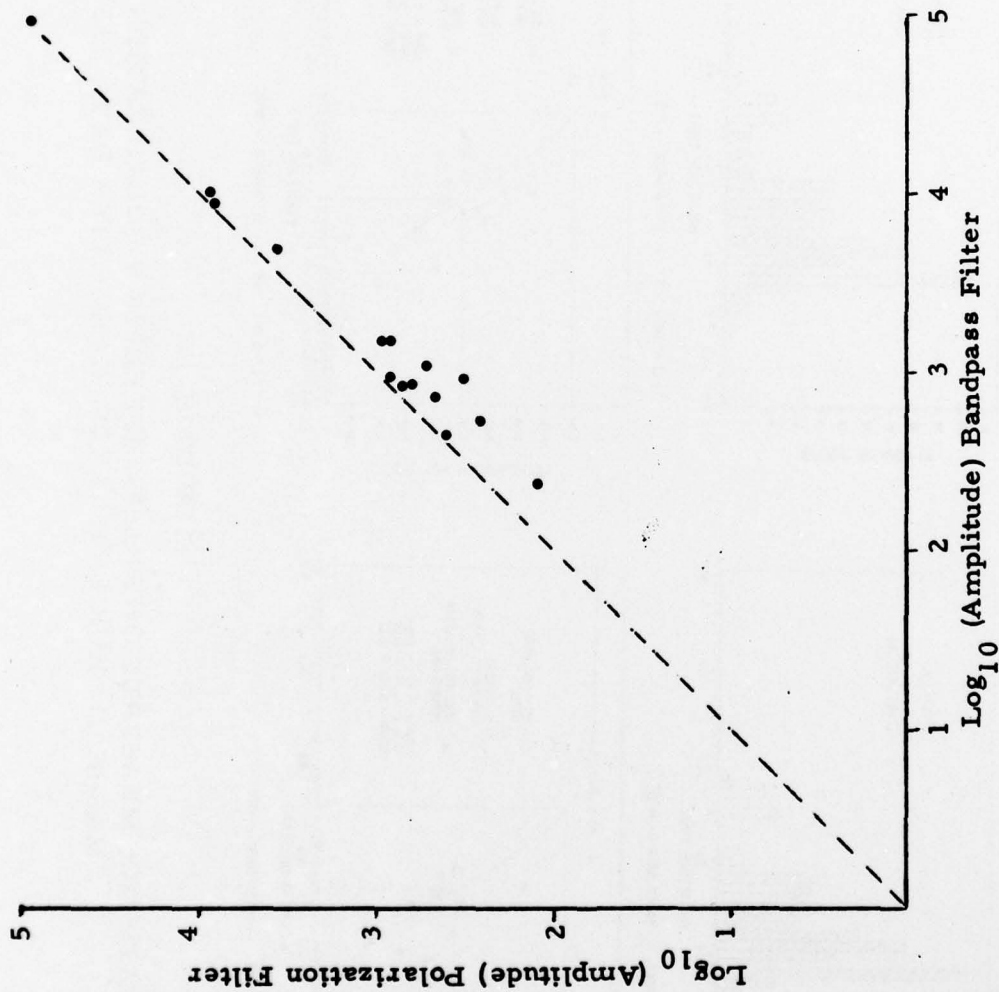


FIGURE III-18

MEASURABILITY OF P WAVES PROCESSED BY THE PHASE-DIFFERENCE POLARIZATION FILTER

data versus peak P wave amplitude measured on the phase-difference polarization filtered data. This plot shows that all P waves suffered some attenuation by the polarization filter, since all points lie below the dashed line. Also, the degree of attenuation appears to increase toward lower values of bandpass filtered amplitude. However, comparison of Figure III-18 with Figure III-10 shows that this form of polarization filter attenuates the P wave signal less than does the particle-motion polarization filter.

E. EXTRACTION OF SHORT-PERIOD SIGNALS BY PHASE-DIFFERENCE POLARIZATION FILTERS

The last part of this study of signal extraction is concerned with the extraction of short-period waveforms by application of the phase-difference polarization filter. Due to time constraints, a full evaluation of this subject was not possible. Therefore, sample results are presented which should indicate the potential value of this technique.

Processing near-field short-period data with the phase-difference polarization filter presented none of the difficulties that the particle-motion polarization filter did, since the phase-difference polarization filter does not require externally derived information (i. e., angles of incidence) as does the particle-motion polarization filter. A sample output of the phase-difference polarization filter is shown in Figure III-19, where the input data is a Kyushu earthquake recorded at the Korean Seismic Research Station with an epicentral distance of 5.84° . Examination of Figure III-19 shows that it is difficult to pick the start time of any phase following Pn on the bandpass filtered traces. After processing by the phase-difference polarization filter, the phases are separated and relatively easy to pick. On the 0° traces, the start of Pg can be picked on the basis of amplitude changes. The following arrivals on these traces appear to be scattered P wave energy. As indicated by arrows on the 90° traces, Lg and Rg start times can be picked on the basis of amplitude and frequency changes. The 180° traces indicate that relatively

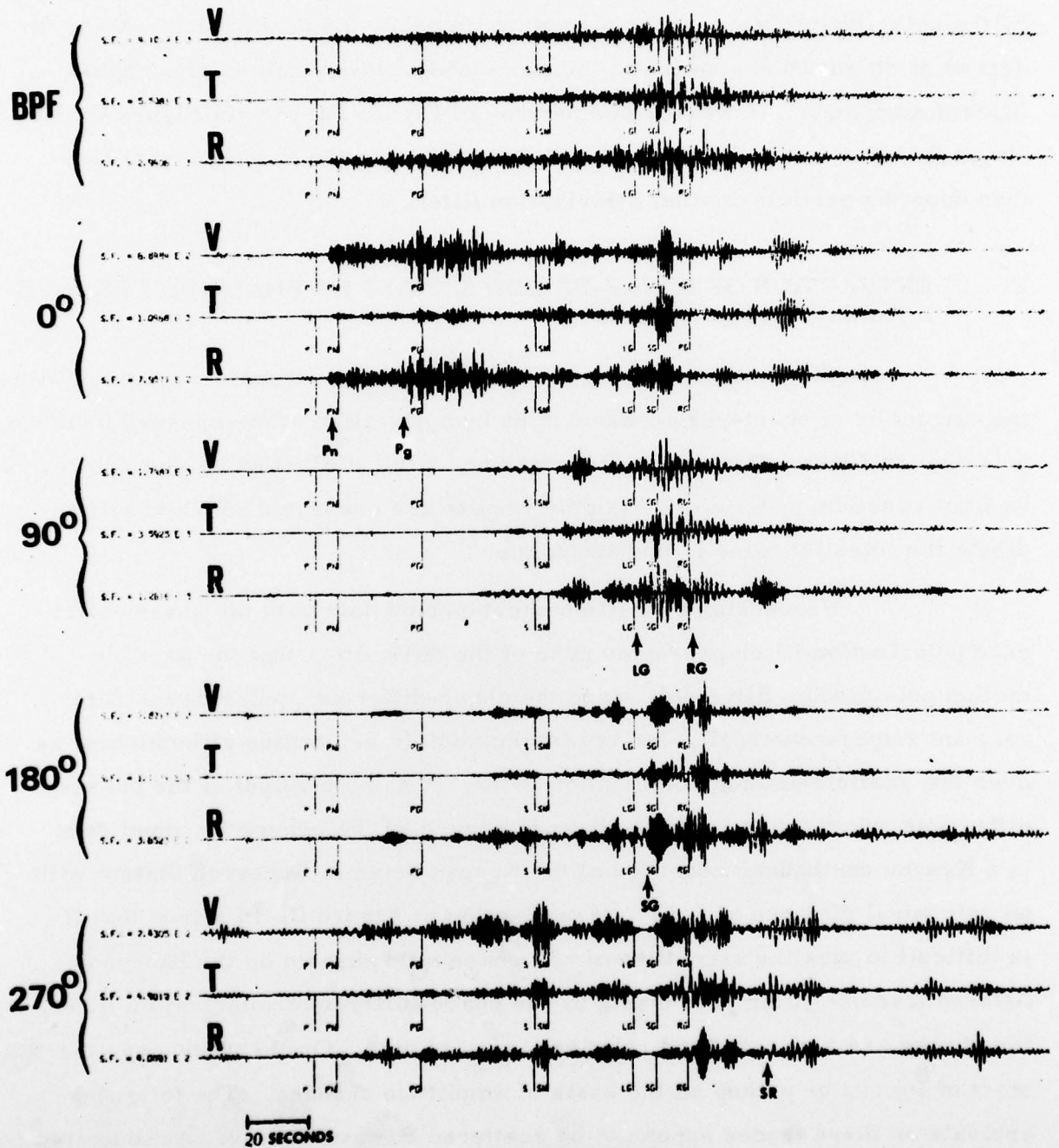


FIGURE III-19

SAMPLE SHORT-PERIOD NEAR-FIELD EVENT PROCESSED
BY THE PHASE-DIFFERENCE POLARIZATION FILTER

little shear energy was released by this event. (Compare the scale factors for these traces with those of the other traces.) No S_n can be picked on these traces, while the S_g arrival appears as one high-frequency burst of energy. The scale factors for the 270° traces show that very little energy of the event is expressed as prograde elliptical particle motion. The most interesting feature on these traces is the waveform starting at the point marked SR, corresponding to a velocity of 2.8 km/sec. This waveform is thought to be a sedimentary Rayleigh wave.

Figure III-20 shows the effect of processing a teleseismic P wave by the phase-difference polarization filter. Comparison of this figure with Figure III-13 shows that the phase-difference polarization filter extracts the P wave as well as the particle-motion polarization filter in terms of noise suppression and produces slightly less signal suppression (2.6 dB average signal loss for the vertical and radial components) than the particle-motion polarization filter (2.8 dB average signal loss for the vertical and radial components).

The preceding brief discussion indicates that the application of phase-difference polarization filters to short-period data will have a twofold benefit. First, this technique allows the extraction of short-period signals from seismic noise, lowering the event detection threshold by some as yet undetermined amount. Second, this technique permits the separation of a short-period signal into its component waveforms, permitting a more detailed study of waveforms obscured on bandpass-filtered traces by other waveforms propagating at nearly the same velocity.

F. FINAL COMMENTS

In this report, two basic types of signal extraction have been discussed. The first type, represented by the Wiener filter-three-component surface wave adaptive processor cascaded combination and the particle-motion

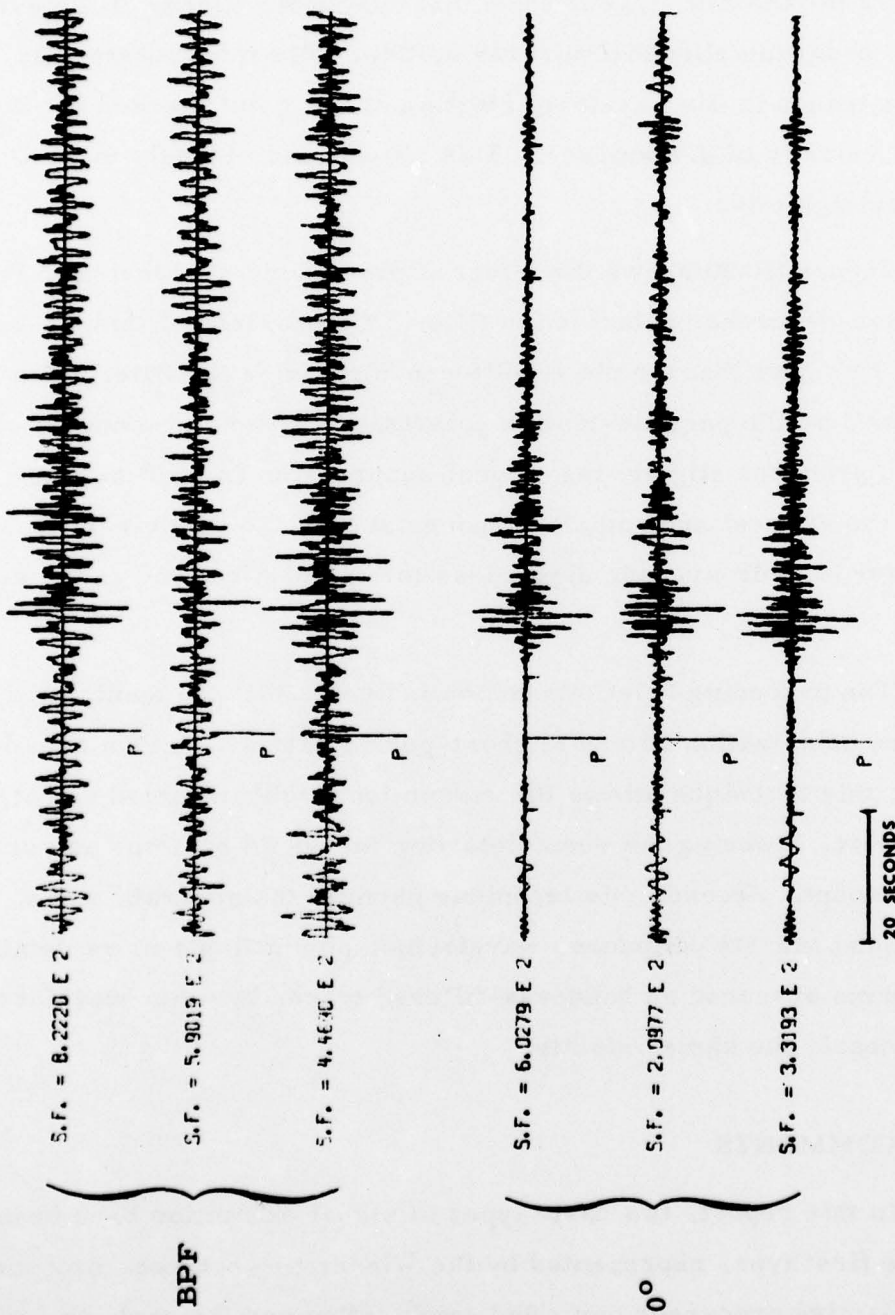


FIGURE III-20
 SAMPLE SHORT-PERIOD TELESEISMIC P WAVE DATA PROCESSED BY THE
 PHASE-DIFFERENCE POLARIZATION FILTER

polarization filter, is highly dependent on information derived from external sources for the quality of its signal extraction performance. The Wiener filter part of the cascaded processor requires a model of the signal (in this case, five signals averaged together) to be extracted, while the particle-motion polarization filter requires good estimates of the bodywave apparent angles of incidence at the recording station. The second type, represented by the phase-difference polarization filter (which includes the bandpass filter-three-component surface wave adaptive processor cascaded combination) is not dependent on information derived from external sources; the only information required is a general knowledge of the signal passband.

The significance of the difference between these two types of signal extraction techniques is that poor estimates of the externally-derived information required by the first type will create distortions of the signal amplitudes so that, while event detection capability may be improved, the magnitudes measured on the processed signals may not be representative of the events which generated the signals. Since the second type of signal extraction technique is basically dependent only on the signal and noise characteristics of the data being processed, this signal amplitude distortion is minimized, permitting the measurement of useable magnitudes. While this second type of signal extraction technique does require knowledge of the appropriate signal passband, this information is easily obtained and is essentially invariant from event to event.

SECTION IV
CONCLUSIONS AND RECOMMENDATIONS

A. CONCLUSIONS DRAWN FROM THIS STUDY

The following conclusions have been reached during the course of the work performed on signal extraction techniques:

- Both the bandpass filter-three-component surface wave adaptive processor and the Wiener filter-three-component surface wave adaptive processor cascaded combinations lower the 50 percent detection threshold by $0.5 m_b$ units.
- Surface wave magnitudes (M_s) measured on data processed by the bandpass filter-three-component surface wave adaptive processor are comparable to surface wave magnitudes measured on the corresponding bandpass filtered data, showing a gradually increasing separation from the surface wave magnitudes measured on bandpass filtered data as m_b decreases. For a given m_b , the variance of these M_s values is approximately the same as the variance of the M_s values measured on bandpass filtered data.
- Surface wave magnitudes (M_s) measured on data processed by the Wiener filter-three-component surface wave adaptive processor are not comparable to surface wave magnitudes measured on the corresponding bandpass filtered data. For a given m_b , the variance of these M_s values is much larger than the variance of the M_s values measured on bandpass filtered data.

- After correction for positive surface wave magnitude bias using Ringdal's technique, the $M_s - m_b$ relationships derived from applying the bandpass filter and the bandpass filter-three-component surface wave adaptive processor have nearly parallel slopes throughout their range of definition from the 25 percent detection threshold to the largest m_b event of the data base.
- The poor performance of the particle-motion polarization filter when applied to Kurile Islands, Kamchatka events as recorded at Guam appears to be due to the station lying near a null in the bodywave radiation patterns and, in the case of shear waves, to distortion of the shear wave particle motion by surface waves.
- When applied to Kurile Islands, Kamchatka events as recorded at Mashhad, Iran, the particle-motion polarization filter produces an improvement in the 50 percent detection threshold of 0.3 m_b units for P and 0.4 m_b units for S.
- Below the 50 percent detection threshold, the attenuation of P wave signals caused by the particle-motion polarization filter becomes significant, making difficult the measurement of long-period m_b for events detected only after being processed by this filter.
- Unless a detailed study of the apparent angles of incidence of P_n , P^* , P_g , S_n , S^* , and S_g is first carried out, it is not feasible to apply the particle-motion polarization filter to near-field short-period bodywaves.
- Preliminary testing indicates that the particle-motion polarization filter may be useful in the extraction of teleseismic short-period bodywaves.

- When applied to long-period bodywaves from Kurile Islands, Kamchatka to Mashhad ($\Delta \sim 66^\circ$), the phase-difference polarization filter improves the 50 percent detection threshold by approximately $0.5 m_b$ units.
- The attenuation of P waves due to application of the phase-difference polarization filter appears to be less than the attenuation due to the application of the particle-motion polarization filter.
- In addition to improving the detection thresholds of short-period and long-period body and surface waves, the phase-difference polarization filter offers the analyst a tool to separate the component phases of a seismogram, making possible more detailed studies of these phases than was previously possible.

B. RECOMMENDATIONS FOR FUTURE WORK

The following points should be considered for any future work using the signal extraction techniques discussed in this report:

- Since the presence in the signal gate of packets of 20-second energy proved to be a strong detection criterion for the cascaded processor surface wave extraction effort, it would be advisable to try narrow-band filtering the data before applying the three-component surface wave adaptive processor.
- A large data base of short-period events should be processed by the phase-difference polarization filter to determine its effect on short-period detection and discrimination.
- It might be fruitful to attempt cascading of the particle-motion and phase-difference polarization filters, since together the models used in these filters completely describe the polariza-

tion of the seismic waveforms. This should have the effect of improving the detection thresholds while decreasing the probability of false alarms.

SECTION V
REFERENCES

- Bullen, K. E., 1965; *An Introduction to the Theory of Seismology*, Cambridge University Press, Cambridge, Great Britain.
- Chandra, U., 1972; *Angles of Incidence of S Waves*, *Bulletin of the Seismological Society of America*, Volume 62, Number 4, pp 903-915.
- Ewing, W. M., W. S. Jardetzky, and F. Press, 1957; *Elastic Waves In Layered Media*, Lamont Geological Observatory Contribution Number 189, McGraw-Hill Book Company, New York City, New York.
- Griffin, J. N., 1966; *Applications and Development of Polarization (REMODE) Filters*, Seismic Data Laboratory Report Number 141, Teledyne Industries Incorporated, Earth Sciences Division, Alexandria, Virginia.
- Jeffreys, H. and K. E. Bullen, 1967; *Seismological Tables*, British Association for the Advancement of Science, London, Great Britain.
- Lane, S. S., 1973; *Evaluation of the Adaptive Three-Component Lamont Processor*, Special Report Number 15, Texas Instruments Report Number ALEX(01)-STR-73-15, AFTAC Contract Number F33657-72-C-0725, Texas Instruments Incorporated, Dallas, Texas.
- Lane, S. S., 1976; *Development of Three Signal Processing Techniques*, Technical Report Number 6, Texas Instruments Report Number ALEX(01)-TR-76-06, AFTAC Contract Number F08606-76-C-0011, Texas Instruments Incorporated, Dallas, Texas.
- Lane, S. S., 1977a; *Extraction of Long-Period Bodywaves*, Technical Report Number 7, Texas Instruments Report Number ALEX(01)-TR-77-07,

- AFTAC Contract Number F08606-77-C-0004, Texas Instruments Incorporated, Dallas, Texas.
- Lane, S. S., 1977b; Extraction of Long-Period Surface Waves, Technical Report Number 8, Texas Instruments Report Number ALEX(01)-TR-77-08, AFTAC Contract Number F08606-77-C-0004, Texas Instruments Incorporated, Dallas, Texas.
- Mereu, R. F., 1965; A Study of Apparent Angles of Emergence at Marathon, Ontario, from the Lake Superior Data, Bulletin of the Seismological Society of America, Volume 55, Number 2, pp 405-416.
- Oliver, J., 1964; Propagation of PL Waves Across the United States, Bulletin of the Seismological Society of America, Volume 54, Number 1, pp 151-160.
- Papazachos, B., 1964; Angle of Incidence and Amplitude Ratio of P and PP Waves, Bulletin of the Seismological Society of America, Volume 54, Number 1, pp 105-121.
- Pho, H. T. and L. Behe, 1972; Extended Distances and Angles of Incidence of P Waves, Bulletin of the Seismological Society of America, Volume 62, Number 4, pp 885-902.
- Poupinet, G. and C. Wright, 1972; The Generation and Properties of Shear-Coupled PL Waves, Bulletin of the Seismological Society of America Volume 62, Number 6, pp 1699-1710.
- Richter, C., 1958; Elementary Seismology, W. H. Freeman and Company, Incorporated, San Francisco, California.
- Ringdal, F., 1974; Estimation of Seismic Detection Thresholds, Technical Report Number 2, Texas Instruments Report Number ALEX(01)-TR-74-02, AFTAC Contract Number F08606-74-C-0033, Texas Instruments Incorporated, Dallas, Texas.

- Ringdal, F., 1975; Maximum Likelihood Estimation of Seismic Event Magnitude from Network Data, Technical Report Number 1, Texas Instruments Report Number ALEX(01)-TR-75-01, AFTAC Contract Number F08606-75-C-0029, Texas Instruments Incorporated, Dallas, Texas.
- Robinson, E. A. and S. Treitel, 1967; Principles of Digital Wiener Filtering, Pan American Petroleum Corporation, Tulsa, Oklahoma.
- Sax, R. L., and C. H. Mims, 1965; Rectilinear Motion Detection (REMODE), Seismic Data Laboratory Report Number 118, Teledyne Industries Incorporated, Earth Sciences Division, Alexandria, Virginia.
- Sax, R. L., 1966; Feasibility of Linear Polarization Measurements for Detecting and Measuring Seismic Bodywaves, Seismic Data Laboratory Report Number 163, Teledyne Industries Incorporated, Earth Sciences Division, Alexandria, Virginia.
- Shimshoni, M. and S. W. Smith, 1964; Seismic Signal Enhancement with Three-Component Detectors, Geophysics, Volume 29.
- Strauss, A. C., 1976; Evaluation of the Improved Three-Component Adaptive Processor, Technical Report Number 7, Texas Instruments Report Number ALEX(01)-TR-76-07, AFTAC Contract Number F08606-76-C-0011, Texas Instruments Incorporated, Dallas, Texas.
- Strauss, A. C. and L. W. Weltman, 1977; Continuation of the Seismic Research Observatories Evaluation, Technical Report Number 2, Texas Instruments Report Number ALEX(01)-TR-77-02, AFTAC Contract Number F08606-77-C-0004, Texas Instruments Incorporated, Dallas, Texas.
- Strauss, A. C., 1978; Application of Ringdal's Method to Unbiased Measurement of the $M_s - m_b$ Relationship, Technical Report Number 15, Texas Instruments Report Number ALEX(01)-TR-78-03, AFTAC Contract Number F08606-77-C-0004, Texas Instruments Incorporated, Dallas, Texas.

Veith, K. F. and G. E. Clawson, 1972; Magnitude from Short-Period P Wave
Data, Bulletin of the Seismological Society of America, Volume 62,
Number 2, pp 435-452.